EXTENDING DEPTH OF FIELD USING A SEQUENCE OF MULTI-FOCUSED IMAGES

Prepared by:

Aadil Volkwin
Vlkaad001

Prepared for:

University of Cape Town
Department of Electrical Engineering

October 2005

Declaration

I, Aadil Volkwin, declare that this thesis is my own work except where indicated.
Any work by other authors has been referenced.

This thesis is submitted in partial fulfilment of the requirements for the undergraduate degree of Bachelor of science in Engineering in Electrical and Computer Engineering at the University of Cape Town, and has not been submitted to any other university or examining body.

Signed: Date:

Acknowledgements

Firstly, I would like to thank Dr. Fred Nicolls for having afforded me the opportunity to conduct my thesis under his supervision, for his willingness to make time and be available.

A big thanks to the MSc students in the DIP lab for their patience in putting up with our presence over the past months, especially Gladys for the use of her coffee mug ☺

To all the 6th floor buddies Brendon, Aaron, Rana, Lisa, Steve, Ken and Mutets whose presence provided an energetic atmosphere during trying times.

To my Volunteers, who took part in my survey necessary to determine the subjective quality appraisals of the resultant images.

To all my friends at U.C.T whose presence in my life has made time here more than just mere experience, each one has made a lasting impact on my thinking and provided me with many a good memory to take forward with me. Special mention to Rana(Joker), Rohith(Mr. Olympia), Jith(The Keeper of the Covenant), Akramus(Prof) and Humz. You've all helped me to find the sunshine in my life ☺ and hope there will always be sunshine in yours. Your trust in my friendship leaves me humbled with nothing more to say than a sincere thank you.

To my darling sister whose endless thought, concern, compassion and encouragement has caused her great financial loss as she walked constantly by me during these last four years.

Finally, I'd like to remember my parents, whose years of sacrifice has enabled me to dream, have and attain opportunities that are unimaginable to the majority of the population on the planet. To them I am truly indebted and dedicate what little I have been able to achieve.

Abstract

This thesis sought to investigate the numerous methods of attaining extended depth of focus with the intention of comparing an implementation of a section of them. This analysis was done against the backdrop provided in the background to the study.

A comprehensive study of the methods relating to an approach consisting of a numerical construction of a single deep focus image from a collection of images obtained by performing mechanical scanning of the specimen on different image planes. An alternative solution based on the use of a specially designed phase plate to use in the optical path that allows an extension of the depth of focus of the images observable was additionally investigated as well as the use of stereoscopic vision and digital holograms.

The result of the investigation revealed a number of possible approaches to resolving the challenge. Of the methods investigated two were implemented and contrasted against *combineZ5* a freely available image processing application designed to enhance Depth of field.

The purpose of such an investigation finds meaning against the backdrop provided by a world of technological evolution and the increased need for ubiquitous, low cost and efficient systems.

Table of Contents

List of Figures

List of Tables

Chapter 1

Introduction

1.1 Subject

This thesis provides insight into the fields of Image processing and Computer vision with specific reference to their application toward the domain of extending depth of field in order to attain Deep Focus.
It seeks to investigate the techniques designed to assemble a composite image, from a sequence of images taken at different focal depths, which is completely free of blurring.

1.2 Background

Umpteen practical applications of computer imaging and machine vision exist. Of these are, surface analysis and fracture detection, auto navigation of unmanned vehicles, studies by entomologists and medical researchers in microscopy to name but a few. These applications make use of optical capturing devices; camera's and light microscopes, the very nature of which result in limited depths of field.

Although a number of techniques and equipment to address the issue of extending depth of field and improving focal range have been developed, the difficulty with these methods are numerous.
Not only are they expensive, they may require a skilled operator or involve time consuming processing stages. Furthermore, in today's modern digital world, where the demand for ubiquity of information and the timeous ease of access to various resources is considered a norm, the implications of these concerns are far reaching. Furthermore due to the nature and complexity of equipment and techniques thus far, it is necessary to have ideas concerning cost, reduction in complexity and increased efficiency and mobility at

the top of research agendas. It is therefore important, for the research and development behind techniques that seek to increase the range of focus of the scenes they capture to be cognisant of these concerns and the development of the increased areas of application of deep focus.

1.3 Objectives

This thesis is geared toward attaining the following objectives:

- Review the origins of depth of field and misfocus.
- Conduct a comprehensive study of the solutions to the challenge of extending depth of focus and therefore image fusion.
- Illuminate the faults associated with image fusion algorithms.
- Establish a means of comparing the performance of image fusion algorithms.
- Compare the performance of various image fusion algorithms.

1.4 Thesis Outline

Chapter 2 provides an introduction to relevant optics related literature and provides insight into the origins of depth of focus, the principles that affect it and efforts to enhance it and finally optics related phenomena that have an effect on the image fusion algorithms.

Chapter 3 introduces the challenge of extending depth of focus from an image processing perspective and provides an understanding of the various paradigms that seek to address the challenge.

Chapter 4 reviews a number of algorithms that pursue the challenge of extending depth of field.

Chapter 5 deals with a variety of methods of combining the final image once the initial challenge of attaining deep focus is overcome. It further delves into defining methods to access the quality of the extended field composites.

Chapter 6 documents the results attained from the algorithms implemented.

Chapter 7 discusses the results and makes conclusions.

Chapter 8 discusses recommendations and future work within the field

Chapter 2

Principles of Optics

This chapter seeks to introduce the field of optics with specific relevance to ***depth of field*** (DOF) and provides insight into image acquisition techniques and the relevant physical issues that endeavor to maximize DOF while illuminating the resultant effects and side effects. It is of significance to determine and understand the stage at which the negative aspects of the side effects begin to outweigh the value of the afore mentioned enhancement techniques. This is of consequence as the final image cannot be of any better quality than the images from which it is composed; therefore promoting the acquisition of a set of high quality images is paramount. [02] Furthermore, the nature of the disparities produced during image acquisition is significant in determining the appropriate fusion algorithm. That being said, there is a definite correlation between the nature of the optics employed, lens design and innovation, image acquisition strategies and the choice of algorithm implemented. Conversely the associated algorithm concerns will affect lens design, hardware limitations, for example processing capability, memory size, cost and energy consumption (in the case of portable devices).

In addition, it provides the basis to explore technical insight into the various algorithms that are geared toward enhancing depth of field through a comprehensive discussion of the algorithms' implementation and image processing approach. This will set up the platform from which to launch discussion surrounding common fusion algorithm faults. This and the following review chapters are a compilation of theory based on numerous sources, which have been appropriately referenced.

2.1 Imaging Properties

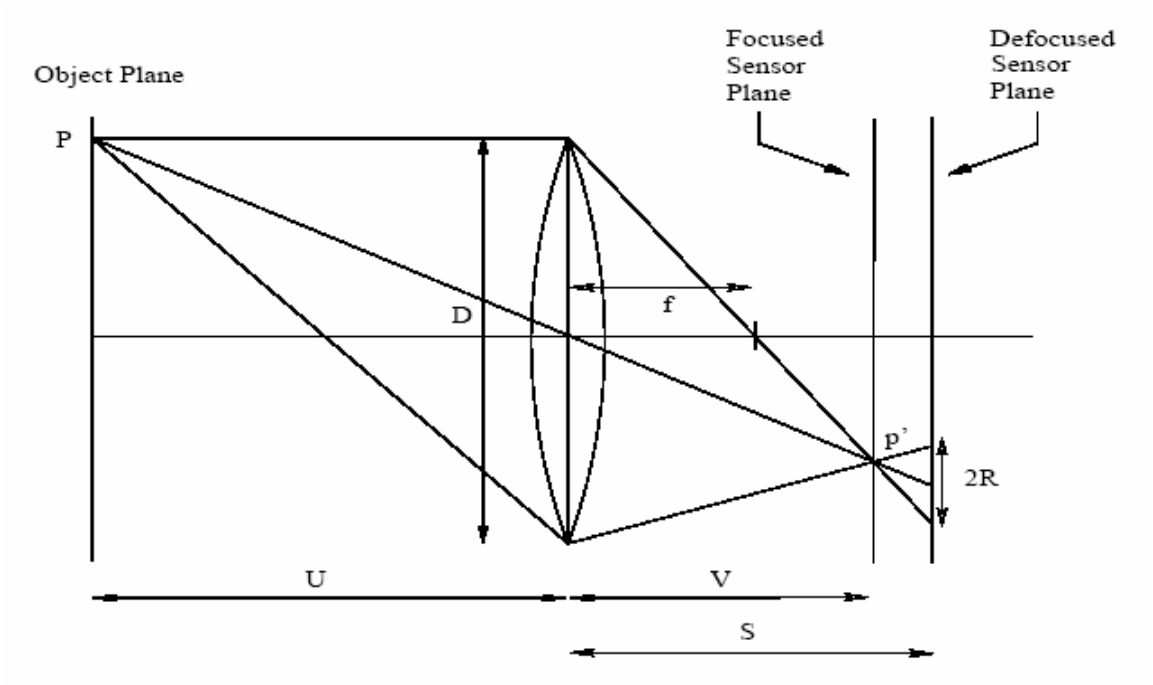

Figure 1: lens construction with typical lengths of interest [01]

A converging lens will focus a beam travelling along the lens axis to a spot (known as the *focal point*) at a distance *f* from the lens. The plane perpendicular to the lens axis situated at a distance *f* from the lens is called the *focal plane*. The plane perpendicular to the lens axis situated at a distance *f* from the lens is called the *focal plane*. Continuing with the thin-lens geometrical model of Figure 1, the point P on the object plane at U in the scene is imaged and perfectly focused as point p' on the image plane at V. The well-known lens equation, $\frac{1}{f} = \frac{1}{u} + \frac{1}{v}$, relates the position of these two points, U and V, with that of the focal length, f, of the lens.

2.2 Depth of Field

When a lens focuses on a subject at a distance, only subjects at that discreet distance in front of the lens is truly sharply focused. Subjects not at that discreet distance are out of focus and therefore theoretically blurry. This is illustrated in Figure.1 below.

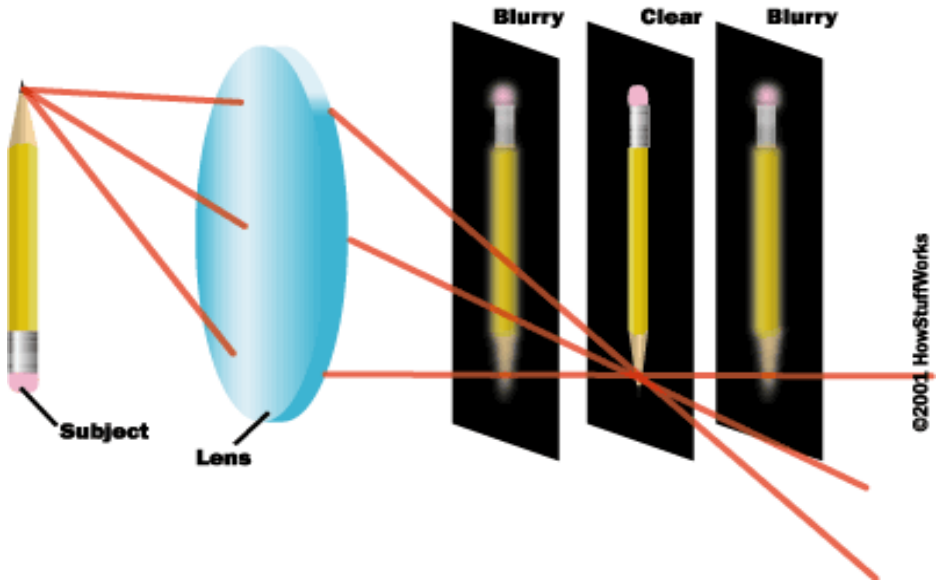

Figure 2: Illustration of image sharpness variance with subject distance from point of focus [23]

However, due to limitations in the human eye, subjects that are slightly nearer to the lens and also subjects slightly further from the lens are perceived to be in focus.

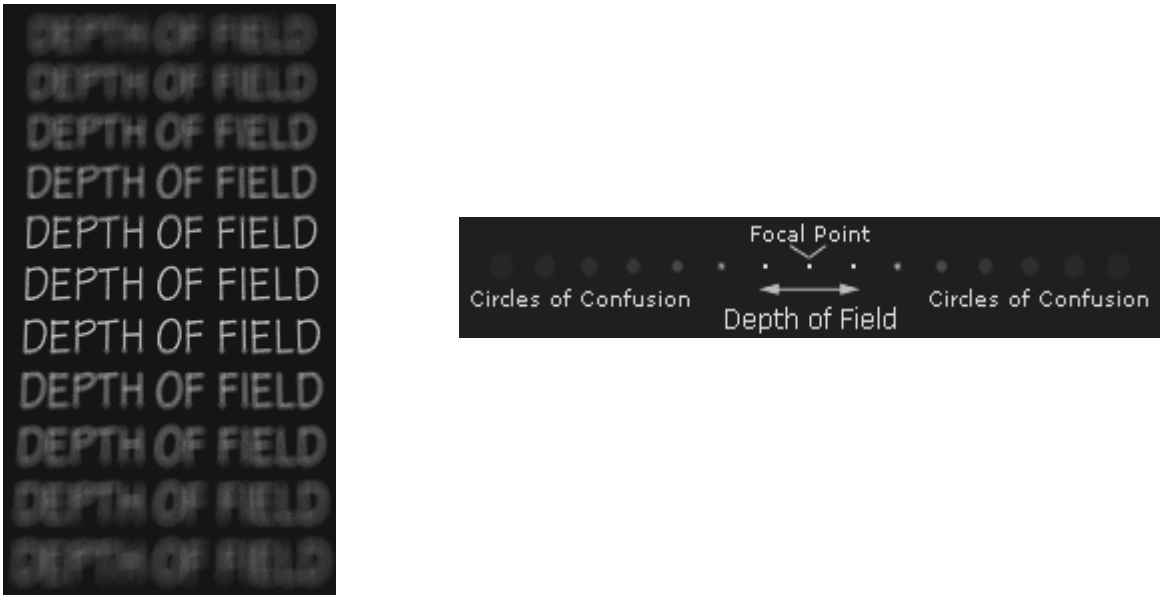

Figure 3: Subjects close to the point of focus appear to be in focus [14]

The entire area of perceived focus is referred to as the ***depth of field*** (DOF). This region is greater behind the point of focus than it is in front, this is due to the angle of light rays changing more rapidly; as they approach being parallel with increasing distance. [18] [24]

At this juncture it is of value to note the distinction between the term ***depth of field*** and ***depth of focus***. Depth of focus is an optics concept regarding the tolerance of placement of the sensor plane, be it film or digital sensor (CCD, CMOS), in relation to the rear element of the lens. While the phrase is sometimes erroneously used to mean depth of field, it should be stressed that *depth of focus* and *depth of field* are ***not*** the same. Depth of field is a measurement of how much distance exists where the subject in the frame will appear to be sharp. Depth of focus, however, is a measurement of how much distance exists behind the lens for a subject to remain sharply in focus. [15]

2.3 Circle of Confusion

The **focus** or **image point** is the point where light rays, originating from a point on the subject, converge [27]. The **principal focus** or **focal point** of a lens is the point onto which light parallel to the axis is focused. Although the focus is conceptually a point, physically, the focus has a spatial extent, called the *blur circle, airy disk* or **Circle of Confusion**.

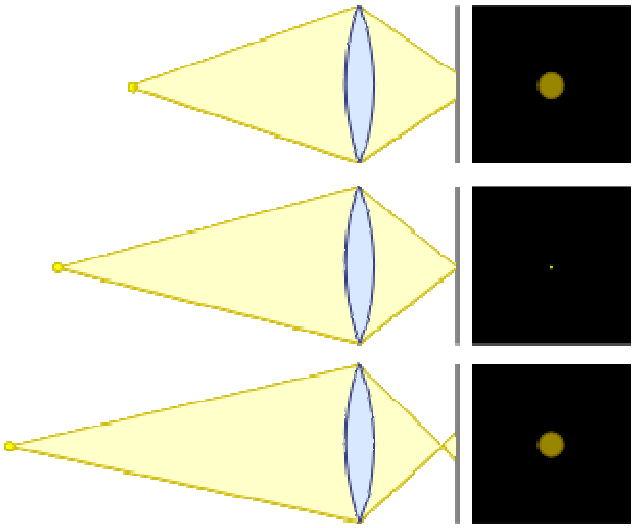

Figure 4: Position of Subject relative to the focal point and corresponding circles of confusion [21]

The depth of field is the region where the size of the circle of confusion is less than the resolution of the human eye. If we can reduce the size of circle of confusion, we can increase the sharpness of the resulting image.

2.4 Image Sharpness

It is tempting to think of sharpness only in terms of focus and depth-of-field however, several factors affect the objective error in focus.

Inclusive are, camera movement, the distance of the subject from the camera, aperture size and the focal length of the lens used.

2.5 Aperture Size and Brightness Variations

In optics, it is that portion of the diameter of an object-glass or mirror through which light can pass free from obstruction. [16]

As a result of circles of confusion being formed by light rays passing through the lens tube, the size of the circles of confusion are directly related to the amount of light that passes through the lens tube, therefore, restricting the amount of light that passes through the tube results in smaller circles of confusion. Restricting the amount of light that passes through the lens is a function of the diaphragm in the lens tube that sets the aperture size. Hence a smaller aperture translates to a smaller diaphragm, which results in less light incident on the sensor plane, film or CCD/CMOS, and smaller circles of confusion, thereby producing a sharper image.[16] [24] [25] [26]

Although reducing aperture size is prescribed as a means to increase a camera system's depth of field, as light rays pass through the lens tube and the diaphragm, some are diffracted. If the aperture is large, the proportion of the diffracted light is small and insignificant, thus in this case, the loss of quality as a result of diffraction is negligible. However, with a small aperture, the amount of light that can pass through the diaphragm is reduced and hence the proportion of the diffracted and non-diffracted light becomes significant. As a result, the quality of the image is also reduced.
Therefore, using small apertures will result in an improved sharpness until a certain point. Thereafter, the quality goes down because of the impact of diffraction.

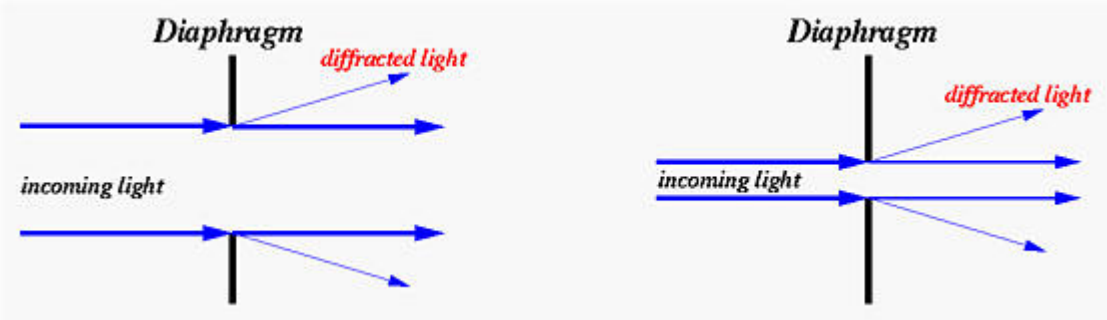

Figure 5: Relationship between aperture size and level of diffraction [24]

Therefore, limiting aperture size is often not an option one can afford as a result of the need to maximise light conditions when imaging in indoor or overcast conditions. Maximising light conditions becomes essential in order to achieve acceptable SNR levels.

Brightness variations are a potential problem for any image fusion algorithm, this being due to uniform patches taken with different focus settings having disparate brightness levels. [01]

2.6 Camera Movement

Decreasing aperture size decreases the amount of light available to expose to the sensing plane, be it film or CCD, therefore resulting in a lack of information reaching this sensory plane and the production of poorer quality images. In a bid to counteract this under exposure, a slower shutter speed is employed.
This increased exposure too has an undesirable side effect; that being that the camera system is sensitive to any motion during the exposure period. Thus, without the use of a stabilizing device, resulting in motion induced blur as illustrated in Figure 6: Motion blur as a result of subject movement during exposure, below.

Figure 6: Motion blur as a result of subject movement during exposure [28]

In addition to this, slight camera movement between frames can lead to the misregistration of images. That being that the features of the subject are not in the same place in each of the frames; which, as well, has an effect on the performance of the fusion algorithms and the quality of the resulting image.

2.7 Magnification

Altering the effective magnification of the imaged object between frames by moving the sensor plane, or more likely the lens, has the unfortunate potential of resulting in an optical phenomenon that poses an obstacle to the fusion of differently focused images, namely misalignment. Change in magnification can be approximated by, see Figure 1: lens construction with typical lengths of interest [01] above, $\frac{1}{S_1} / \frac{1}{S_2}$ where S_1 and S_2 are the respective sensor to lens distances of each frame. Consequently we can normalize the images using the corresponding $S_{i's}$ for each image to rescale them appropriately. Despite this rescaling, alignment problems due to blur and the change in lens position do still occur. Thus the algorithm of choice must be tolerant of this. [01] Furthermore, working at high magnification can result in snowy or grainy images.

2.8 Aberrations

Lenses do not form perfect images, and there is always some degree of distortion or *aberration* introduced by the lens which causes the image to be an imperfect replica of the object. Careful design of the lens system for a particular application ensures that the aberration is minimised. There are several different types of aberration which can affect image quality

2.8.1 Spherical aberration

Spherical aberration is caused because spherical surfaces are not the ideal shape with which to make a lens, but they are by far the simplest shape to which glass can be ground and polished and so are often used. Spherical aberration causes beams parallel to but away from the lens axis to be focused in a slightly different place than beams close to the axis. This manifests itself as a blurring of the image. Lenses in which closer-to-ideal, non-spherical surfaces are used are called *aspheric* lenses, which are complex to make and often extremely expensive. [21]

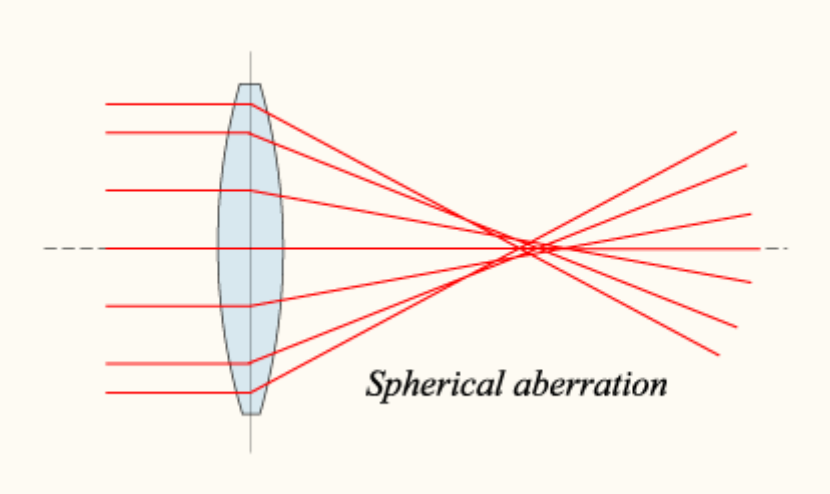

Figure 7: Spherical aberration [21]

The figures below depict spherical aberration in an optical system with a circular, unobstructed aperture admitting a monochromatic point source. Inside focus is to the left, and outside-focus is to the right, light is propagating from left to right.

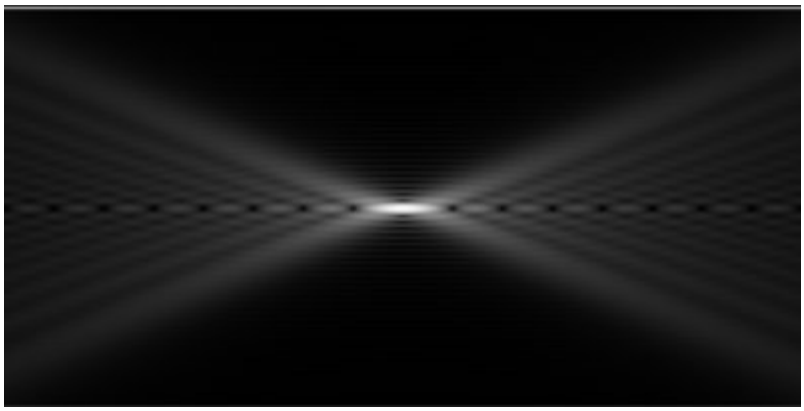

Figure 8: Longitudinal sections of spherical aberrations through the focus.

Figure 9: Spherical aberration in the focal plane.

2.8.2 Coma

Light rays incident to a lens with focal length f at an angle θ to the axis are focused to a point f tan θ distance away from the optical axis. Rays passing through the outer margins of the lens are focused at different points, either further from the axis (positive coma) or closer to the axis (negative coma). A beam of parallel rays passing through the lens at a fixed distance from the centre of the lens are focused to a ring-shaped image in the focal plane, known as a *comatic circle*.

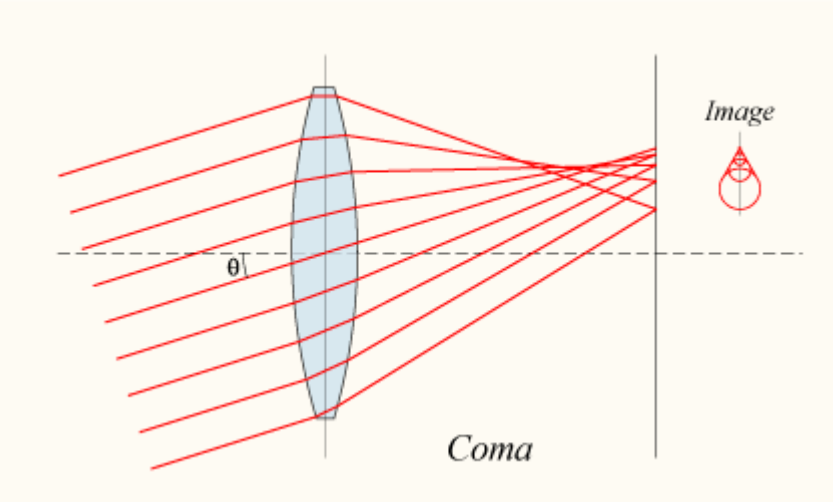

Figure 10: Coma aberration

2.8.3 Chromatic aberration

Chromatic aberration is caused by the dispersion of the lens material, the variation of its refractive index n with the wavelength of light. Thus different wavelengths of light will be focused to different positions. Chromatic aberration of a lens is seen as fringes of colour around the image.[21]

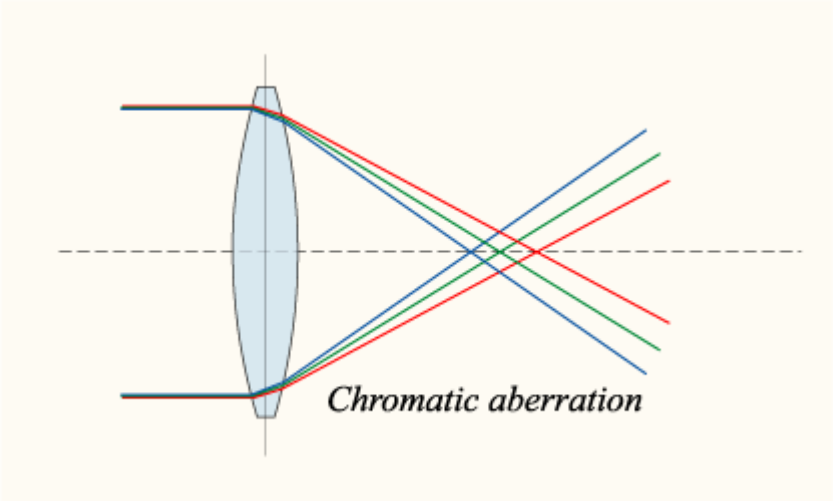

Figure 11: The different wavelengths are focused at different points on the axis

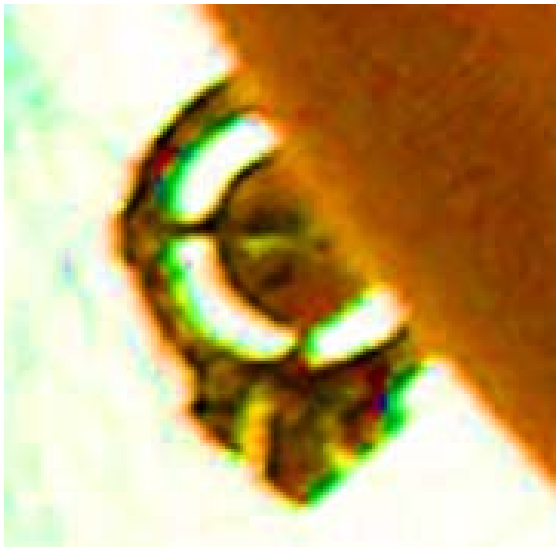

Figure 12: Photographic illustration of chromatic aberration

Chapter 3

Algorithm Analysis

Image fusion involves selecting different regions from a sequence of images and pasting them together in one image. The regions are selected on the basis of special properties that they posses. This chapter investigates this process.

Numerous articles have been produced relating to image fusion, documenting a variety of approaches to tackling this challenge. These techniques can be classified into four main types. [01] [02] [03] [04] [07] [08] [09]

- Pixel variance
- Edge detection
- Contrast measurement/energy gradients
- Information content/signal processing solutions

Although most algorithms and their variations fall into any of the four above categories, there exist alternative approaches. The final part of this chapter describes some interesting alternative paradigms.

The basic approach of the algorithms is as follows:

1. Initially a series of p images slices, I_p, are obtained by serially stepping the microscope through a fixed small step using the optical axis focus controller.

2. The aim is to assemble a composite image by returning a selected pixel at every pixel location or small image region depending on the algorithm (the size of the composite image is the same in all the image slices) corresponding the best in-focus material across all slices at that pixel location.

3. For all image slices I_k:$k = 1 \ldots p$, every pixel is scanned and for every pixel

($I_p(i,j)$ $i = 1 \ldots N$ and $j = 1 \ldots M$ for an image of dimension $N \times M$.) location a measure is made for every slice at the corresponding location on how in-focus the slice region appears at the pixel location.

4. The selected pixel is chosen by the evaluation of the function that returns some measure of likelihood of the pixel being in focus. The main difference in the algorithms below is in how they formulate this measure. Some use a point process, others work on an area and others work in the frequency domain.

Thus essentially every pixel is scanned and for every pixel location a measure is made for every slice at the corresponding location. The candidate pixel with the best measure is then selected, according to criteria laid out for each algorithm below. [05]

This classical approach, which is the basis for the following algorithms, suffer, apart from algorithmic deficiencies/inaccuracies, from a lengthy image acquisition process which posses a challenge to acquiring deep focus images for dynamic objects.

3.1 Pixel Variance

Pixel based fusion is modelled on two approaches. A point based image fusion and Neighbourhood based image fusion. In the point based approach pixels with the same coordinates are compared in all Z images of a stack. A minimum or maximum rule is then applied to select the best pixel in focus.
In the second case, the algorithm is based on the assumption that the larger intensity variations occur in a region surrounding the pixel. Thus the pixel along the Z axis with the biggest variance to its surrounding pixels will be selected for the composite image. This algorithm is computationally simple but susceptible to brightness variations which are addressed by normalising the variance across the image first. [01] [02] [05]

3.2 Edge Detection

Edge detection makes use of the concept that focussed images have a high intensity and therefore a large change in luminance values between nearby pixels once the image has been appropriately filtered. A number of filters are available to do this including the Sobel edge detection operators and the Laplacian filter. These changes, however, disappear as the edges blur in a poorly focussed image. Therefore applying an edge detection filter to the image and then accumulating the differences between adjacent pixels should result in a large value if there is a strong edge or a low value if the edge is blurred.

These methods add some overheads in that the filtered versions of the images have to be computed and stored, but once this is done, calculating the measure only involves simple integer arithmetic and is therefore fast. [02]

3.3 Contrast and Energy Gradients

As with edge detection the argument that sharply focussed images have greater energy levels than do poorly focused images. The contrast is measured as the difference in luminance values between neighbouring pixels. Various measures based on this approach have been proposed and have the advantage of being very fast to compute since they involve only simple subtractions of luminance values. [02]

3.4 Multiresolution based approach

The crux of this approach is based on the knowledge that in focus parts of an image contain many details and therefore high frequency components. Firstly input images are decomposed using a multiresolution technique. Extending the depth of field follows from the application of an area based selection criterion and finally a consistency verification step.

A method used in this approach is to use Fourier analysis and the Fast Fourier Transform (FFT). However the FFT is not considered ideal. The theoretical basis of FFT is that the

signal that is being analysed is periodic and thus is described as the sum of a set of sine and cosine functions. However, real world signals are rarely periodic and do not repeat indefinitely thus important features in the signal occur briefly and unpredictably. Images can be considered as non-periodic signals and their important features are analogous to brief spikes. [02] [04] [05]

In recent years, there has been much interest in a related technique, the Discrete Wavelet Transformation. Mathematically it is very similar to the Fourier Transform except that the underlying basis functions are not sine and cosine, but instead, are an infinite set which can be of short or long duration.

The term wavelet is defined as small wave; therefore any function that is a wavelet is a wave with small characteristic amplitude. Furthermore the amplitude of the wave decays as the distance from the centre of the wave increases. This property lends itself to the manipulation of a spatial localisation and therefore has high saliency detection as it supports the local analysis of an image's frequency content. Furthermore, it has frequency characteristics similar to the Fourier transform. A distinguishing feature of the wavelet transform over the Fourier transform is that it adapts to various sizes of details. The above properties are both exploited in the extended depth of focus processing. The frequency properties of the wavelet transform are exploited to perform high pass filtering, as in-focus material will give rise to high-frequency data in the transform.

In order to perform a wavelet transform of an input signal, a family of wavelets is created from dilations and translations of a prototype ψ that for a one-dimensional function in the discrete version can be defined by:

$$\psi_{m,n}(i) = 2^{-m/2}\psi\left(2^{-m}i - n\right)$$

at resolutions separated by a factor of 2 and m and n being integers. The wavelet decomposition is then:

$$f(i) = \sum_{m,n} c_{m,n}\psi_{m,n}(i)$$

and ψ chosen such that $\psi_{m,n}(i)$ constitute an orthonormal basis.

Similarly, a scaling function is introduced as:

$$\phi_{m,n}(i) = 2^{-m/2}\phi\left(2^{-m}i - n\right)$$

Again, the $\phi_{m,n}(i)$ are orthonormal for fixed m.
In the case of a 2D function (an image) the scaling function is:

$$\phi(i,j) = \phi(i)\phi(j)$$

The decomposition at each resolution is given by three wavelets:

$$\psi^1(i,j)=\phi(i)\psi(j)$$

$$\psi^2(i,j)=\psi(i)\phi(j)$$

$$\psi^3(i,j)=\psi(i)\psi(j)$$

The set of wavelet coefficients typically used are Harr, Daubechies
Harr wavelet basis functions are frequently used in image compression algorithms. However, the Daubechies, A computationally efficient technique, functions offer a smooth (orthonormal and compact) basis for the computation of wavelet transforms. Implementations of this format are not uncommon and have become the function of choice in many Image processing applications. [05] [08] [09]

3.5 Variations from the Norm

This section looks at three alternatives to the traditional methods described above.

3.5.1 Wavefront Coding

Wavefront Coding is a general technique used to greatly increase imaging performance while also reducing the size, weight, and cost of imaging systems. Wavefront Coding combines non-rotationally symmetric aspheric optical elements and digital signal

processing in a fundamental manner to vastly extend the depth of field of imaging systems. Wavefront Coding optical elements are phase surfaces and as such do not absorb light or increase exposure or illumination requirements. Misfocus related aberrations that can be controlled with Wavefront Coding include chromatic aberration[2], Petzval curvature, astigmatism, spherical aberration[3,4], and temperature related misfocus.

The signal processing used is dependent on the specific optical system. The Wavefront Coded optics are dependent on the type and amount of signal processing to be used. Since the optics and signal processing are closely coupled, it is natural to expect best performance from systems where the optical and digital components of the system are jointly optimized during design.

The digital components are designed to minimize algorithm complexity, processing time, and effects of digital processing on image noise. [10] [11]

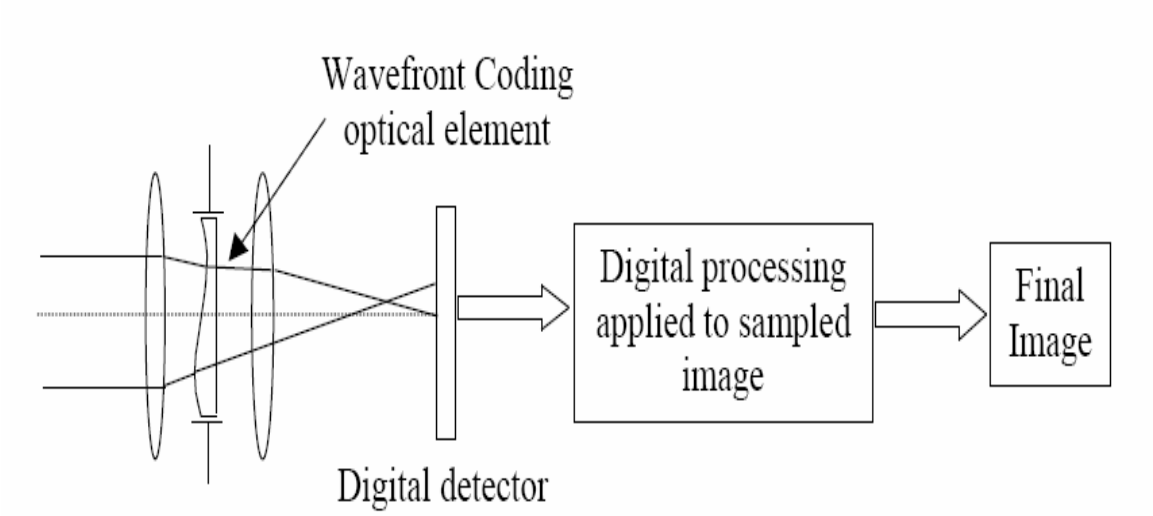

Figure 13: Block diagram of a wavefront coding imaging system

The following figure provides an understanding of the manner in which light is affected and manipulated by the particular wavefront coded system optics. It further draws

distinction between the more traditional optic systems and wavefront coding, illustrating the systems lack of sensitivity to misfocus.

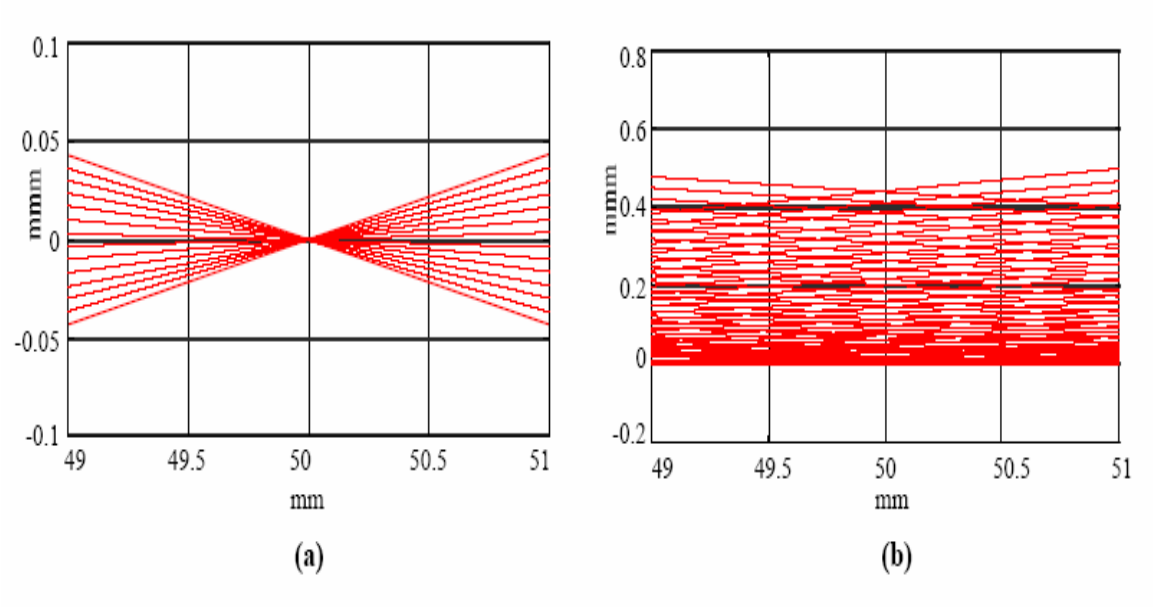

Figure 14: Ray diagram illustration of wavefront coding

Finally the Figure below further demonstrates the wavefront coded systems lack of sensitivity to misfocus related aberrations by illustrating the effect of misfocus on the Point Spread Spectrum (P.S.F) of a traditional optical system and comparing it to the P.S.F of wavefront coded sytem. A clear distinction lies between the effect of misfocus on a traditional systems focused P.S.F and that of a wavefront coded systems focused P.S.F

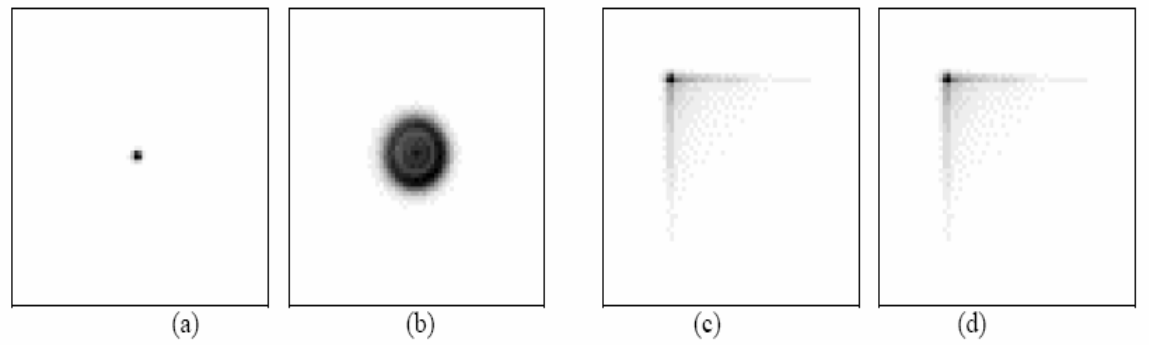

Figure 15: Comparison of Point spread spectrums of traditional imaging optics and a wavefront coded system

This method however is limited in that it is necessary for the additional optics (wavefront coding optical element) to be specifically designed and fabricated as a function of the specific object and of the specific kind of adopted optical system.

3.5.2 Stereoscopic Imaging

Credible Literature on this topic has proven challenging to come across, hence the details are to some extent “sketchy”. However mention is made here of the approach as it does provide insight and understanding of the variation and possible innovation that still lies untapped.

Software that performs a 3 D reconstruction of images works by inputting a photo of a specimen and then inputting a second photo of the same specimen shifted left or right slightly. The result is viewed through a pair of stereoscopic glasses.
However, if instead of moving the specimen to take the second shot, refocus the camera and capture a deeper slice of the specimen. The software can then use the two separately 'focused' images to construct a deep-field image, once more, viewing the image produced through stereoscopic glasses. [29]

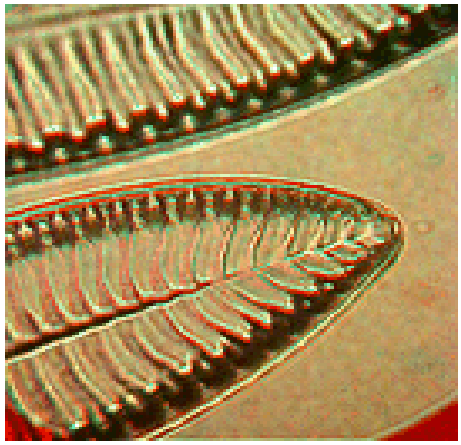

Figure 16: Viewed through stereoscopic glasses produces a deep focused image

3.5.3 Digital Holograms

Actually, two approaches exist to obtain an extended focused image, both having severe limitations since the first requires mechanical scanning while the other one requires specially designed optics.

The literature reveals that it is possible to obtain an extended depth of field image without any mechanical scanning as we have seen is necessary in micro and macro photography or the use of specially designed optics as is the case with wavefront coding.

Chapter 4

Sample Algorithm Implementation

From the previous chapter, it is seen that there exists a number of approaches to solving the issue of extending depth from focus. As expected a plethora of implementations, variation of implementations and innovations have been developed and experimented with and there continues to be further research and development in this field.
This Chapter serves to illuminate some of the implementations of the named approaches that exist out there.

4.1 Point based Pixel Variance

4.1.1 Algorithm 1

A function evaluating the distance from the mean of maximum and minimum values in a series of slices. This is referred to as index Q which uses the |maximum−average| − |minimum−average| as the decision function:

$$Q(i,j) = |I_{\max}(i,j) - \overline{I_p(i,j)}| - |I_{\min}(i,j) - \overline{I_p(i,j)}|$$

where

$$I_{\max}(i,j) = \text{maximum}[I_1(i,j), I_2(i,j), \ldots I_p(i,j)],\ I_{\min}(i,j) = \text{minimum}[I_1(i,j), I_2(i,j), \ldots I_p(i,j)]$$

and $\overline{I_p(i,j)}$ is the intensity average taken over the set of image slices. If $Q(i,j) \geq 0$ then the value chosen for the composite image will be $I_{\max}$ otherwise if $Q(i,j)<0$ then $I_{\min}$. The composite image is built with the $I_{\max}$ or $I_{\min}$ selected pixels from the set of slices for each image pixel. [05]

4.2 Area based Variance

4.2.1 Algorithm2

A nondirectional difference operator, index *D*. For every corresponding pixel location across all *k* slices, $k = 1 \ldots p$, a measure D_k is computed:

$$D_k(i,j)=|I_k(i-1,j+1)-I_k(i+1,j-1)|+|I_k(i+1,j+1)-I_k(i-1,j-1)|+|I_k(i,j+1)-I_k(i,j-1)|+|I_k(i-1,j)-I_k(i+1,j)|$$

The image closest to focus at pixel (i,j) will satisfy:

$$D_{\max}(i,j) = \text{maximum}[D_1(i,j),D_2(i,j),\ldots D_k(i,j),\ldots D_p(i,j)]$$

The composite image is built in a manner similar to algorithm 1, where the pixel corresponding to the selected $D_{\max}$ value is selected.

In both cases the procedure implies taking the differences between the gray levels of pairs on nearby pixels in each optical slice. Differences are compared for corresponding coordinates in all the slices in the stack and the set that present the higher difference is selected for the composite image.

4.2.2 Algorithm 3

This is an area algorithm based on a 5×5 kernel which selects pixels for the composite image in terms of a maximum function of local area focus.

$$V_{ext}(i,j,p) = \frac{\sum_{l=-2}^{+2}\sum_{m=-2}^{+2}(V_k(i,j,p) - V(i+l,j+m,p))^2}{V_k^2(i,j,p)}$$

$$V_k(i,j,p) = \frac{1}{25}\sum_{l=-2}^{+2}\sum_{m=-2}^{+2} V(i+l,j+m,p)$$

The maximum of $V_{ext}(i,j,p)$ fixes the position of the focused area and contributes to the composite image by selecting the image pixel value corresponding to the position of the maximum $V_{ext}(i,j,p)$ for every pixel in the image.

4.3 Edge Detection

4.3.1 Algorithm 4

The Sobel operator is employed to select the best in-focus slice. Essentially the Sobel operator is an edge detector with some noise smoothing incorporated. The Sobel operator returns a measure of the strength of an edge being present at a given pixel. Clearly in-focus regions will have strong edges present. The composite image is composed by selecting the pixel with the corresponding strongest (maximum) edge value through the set of slices for the pixel coordinates. The process is repeated for every pixel in the composite image.

4.4 Multiresolution based approach

4.4.1 Algorithm 5

Images are partitioned into square blocks of 8×8 pixel size. Each image is high pass filtered by $\left(\delta(i,j)-h_{gtr}(i,j)\right)$,where δ, the 2D discrete delta function $\delta(i,j)$is 1 if $(i,j) = (0,0)$ and 0 otherwise, and $h_{gtr}(i,j)$is a truncated Gaussian function defined as:

$$h_{g_{tr}}(i,j)=\begin{cases} C\exp\left(-\dfrac{i^2+j^2}{\sigma_g^2}\right) & \text{for } |i|\le l_1 \text{ and } |j|\le l_2 \\ 0 & \text{otherwise} \end{cases}$$

where C is a normalization constant, σ_g^2 is the variance of the Gaussian distribution and l_1 and l_2 are the integers to restrict the nonzero region of $h_g(i,j)$. Suggested values are $\sigma_g^2=20.0$ and $l_1=l_2=7$. The energy index in the (i,j)th block is given by:

$$e_{p,(x,y)}=\sum_{i=xM}^{(x+1)M-1}\sum_{j=yM}^{(y+1)M-1}\left(C(i,j;l_1,l_2;S)\sum_{m_1=-(l_1-1)/2}^{(l_1-1)/2}\sum_{m_2=-(l_2-1)/2}^{(l_2-1)/2}h_{g_{tr}}(m_1,m_2)I_p(i-m_1,j-m_2)\right)^2$$

where:

$$C(i,j;l_1,l_2;S)=\left(\sum_{m_1=-(l_1-1)/2}^{(l_1-1)/2}\sum_{m_2=-(l_2-1)/2}^{(l_2-1)/2}h_{g_{tr}}(m_1,m_2)^{-1}\right)$$

where S is defined in the image domain as:

$$S=\{(i,j)\,|\,0\le i\langle M;0\le j\langle M\}$$

and $m_1 = m_2 = 8$

In-focus areas in an image clearly give rise to sharp edges in an image. When transformed into frequency space sharp edges give rise to high frequency components. Therefore the effect of high pass filtering is to attempt to remove (low frequency) out of focus data. The block with the maximum energy in each subset of corresponding blocks in the stack of images is selected for the composite image. The algorithm derives its methods from Fourier theory even though the actual implementation operates in the spatial domain.

4.4.2 Algorithm 6

The following algorithm (Forster et al., 2004) [04] exploits the effects of wavelet transforms. It is of elevated interest as it serves as an illustration of the ongoing development of existing techniques, as mentioned in the chapter introduction, by making use of *complex wavelet transforms*.

A flowchart outlining the procedure is shown below and consists of the following steps:

1. Vector-to-scalar conversion: multichannel (e.g. colour image) data is converted to one channel.
2. Complex-valued discrete wavelet transform.
3. Applying the selection rule and consistency checks.
4. Inverse complex-valued discrete wavelet transform.
5. Scalar-to-vector conversion: reassignment to obtain multichannel data.

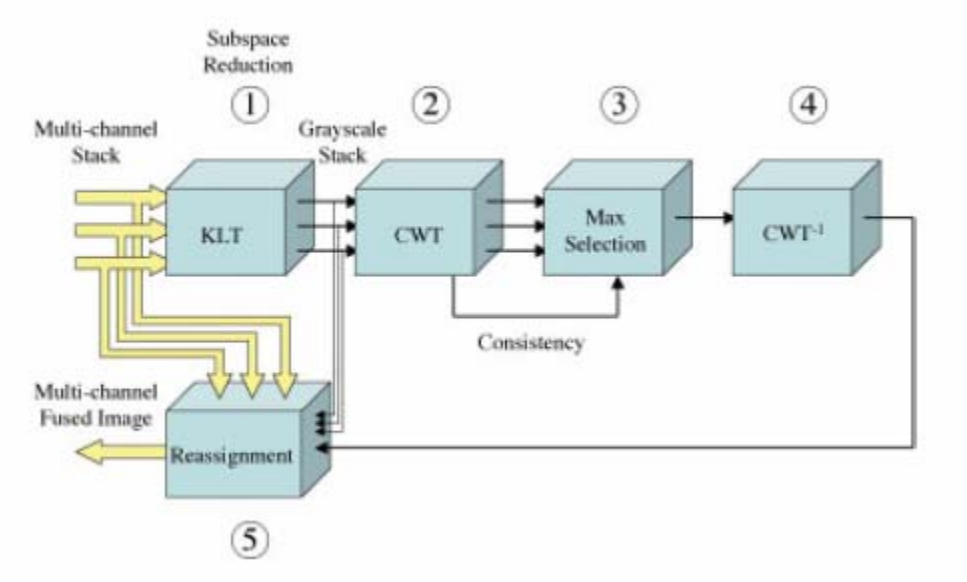

Figure 17: Complex wavelet image fusion algorithm

Steps 2 and 4 represent the core of the image fusion algorithm and are thus the object of particular interest here.
In an effort to determine the regions of greatest focus the wavelet transform is employed in order to decompose the image into subbands that contain details of varying sizes. Large wavelet coefficients, produced as a result of the wavelet transform, indicate the presence of pronounced detail at the corresponding points.

The proposed wavelet transforms are orthonormal basis decompositions and thus the information in the different wavelet subbands is unique and therefore nonredundant, not withstanding that the wavelet transform algorithm relative to alternative multiresolution techniques has a computationally fast algorithm.

The algorithm employs the use of complex Daubechies wavelet bases as a number smoothness orders are available and in this case four are implemented which is useful in implementing an additional noise reduction step. The complex-valued wavelet transform is formed by filtering with finite-length complex low and high pass filters, h and g, and downsampling thereafter, as shown in the figure below.

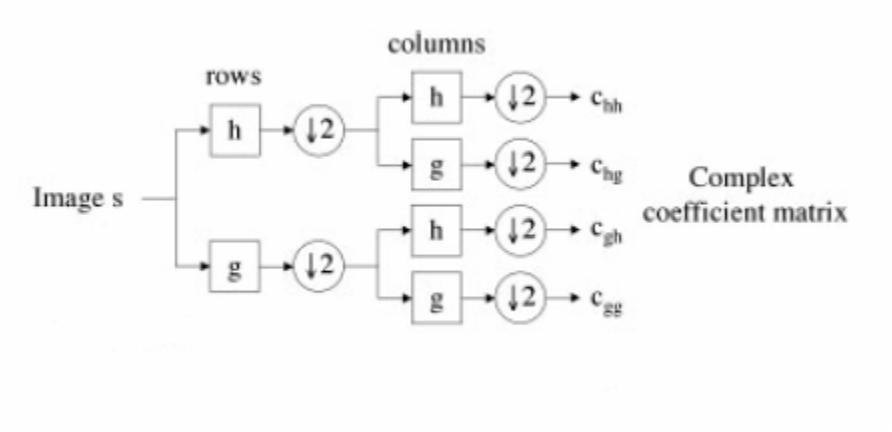

Figure 18: Decomposition of an image by complex wavelet transform

Thus, the first step of the algorithm is to perform a 2D separable complex wavelet transform CWT:

$$\text{CWT}: \quad s(x,y;z) \longrightarrow \{c_j(n,m;z)\}_j$$

for each slice $s(.,.;z)$ of the stack $\{s(x,y;z)\}_z$ which yields complex-valued coefficients c_j for each scale j and all z. The complex-valued transform adds robustness to the selection rule and consistency check algorithms, due to the fact that the selection operator only takes into account the absolute value of the coefficients, and keeps the phase unchanged. The phase of the wavelet coefficient is interpreted as the carrier of detail information, whereas the amplitude weights this information.

Step 3 of the algorithm is built on the premise that the largest absolute values of the coefficients in the subbands correspond to sharper brightness changes and therefore the most salient features as elucidated by the following formula.

$$d_j(n,m) = c_j\left(n,m;\text{argmax}_z\left|c_j(n,m;z)\right|\right)$$

As a spatial consistency check, if the majority of neighboring numbers in a 3 x 3 window of a matrix containing the wavelet coefficients, from d above, are from a different slice $k \neq j$, then the number $M(n,m)$ j is changed to $M(n,m)$ k, and the respective coefficient is adapted: $d_{j,new}(n,m) = c_j(n,m,k)$.

Step 4 performs the inverse complex wavelet transform, thereby tackling the issue converting the fused coefficient matrix to obtain an intermediate fused image. This is depicted mathematically by the following formula.

$$CWT^{-1} : \{d_j(n,m)\}_j \longrightarrow p(x,y)$$

In general, the pixels of the reconstructed image are complex numbers. Two schemes for mapping these back to real values are considered:

1) Calculating the absolute value of the complex number per pixel

2) Taking the real part of each pixel.

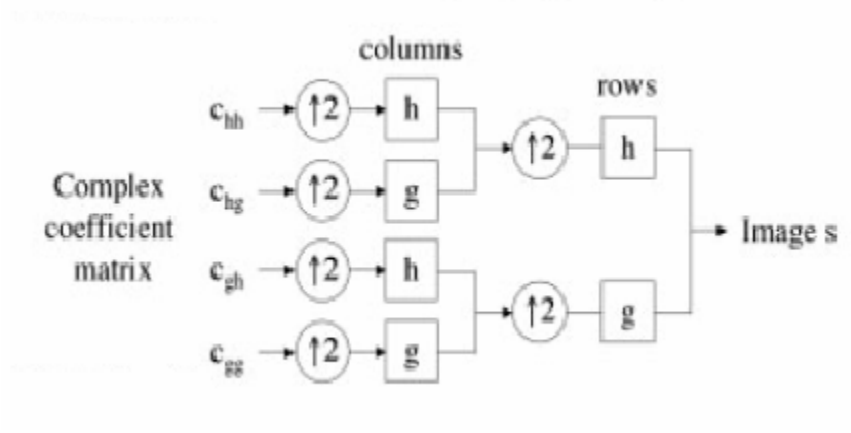

Figure 19: Reconstruction of complex coefficient matrix to composite image

Chapter 5

Image Combination and Comparison Techniques

Simply combining the pixels with the highest value, for the chosen measure of focus, tends to lead to sharp transitions in the final image which may be visible as edges or lines. Furthermore, even if the discontinuity between image regions is negligible, the overlapping blur at focus boundaries makes all fusion algorithms susceptible to uncertainties in assigning the precise region boundary to the resultant map. Objects in the background regions are blocked by foreground objects to the extent of their circle of confusion radius. Unfortunately, neither image in the pair contains a focused representation of this occluded region. [02]
Furthermore, it will describe several methods of comparison commonly used in industry to compare the result of the fusion algorithms. The concepts described in this chapter will be used to justify algorithm comparisons.

5.1 Image Combination Techniques

The Figure below illustrates the effects of using different combination techniques. The Image on the left, using simple combination, sufferes from the halo effect around the queen and within the squares of the chess board. The Image on the right, using a weighted average, has less pronounced haloing.

Figure 20: The result of using different combination techniques, the Image on the left suffers from the 'Halo' effect

5.1.1 Simple Maximum

This combination method simply selects the pixel for which the focus measure is greatest. It tends to suffer from “halo” effects where areas of plain colour are close to a sharp edge and may also suffer from “mottling” in large areas of plain colour. Its main advantages are that it is easy to understand and quick to compute.

5.1.2 Weighted Average

This attempts to use more of the information available from a consideration of how the focus measure for a particular pixel changes across the frame stack and also applies a degree of smoothing. A weighted average frame number is calculated for the same image patch as used for calculating focus measures. The weight is calculated by dividing the maximum value of the focus measure by the number of parts in focus. So, in this way patches with a higher number of possible focal points (more blurry) the weighting of its influence on the final image is reduced, which tends to reduce the “halo” affect.

5.1.3 Key Frame below Threshold

This method works by using the most focussed image, the key frame, as a base upon which to build the final. Pixels from other images are replaced from others when they have a sufficiently larger focus measure.
A threshold is decided by considering the maximum values for the focus measure for each pixel. These are sorted and the value that is exceeded by 40% of pixels is found. If the maximum value for the focus measure for a given pixel is above this threshold in an image other than the key image, then that pixel is replaced; otherwise the pixel from the key image is retained.

5.1.4 Propagate

This combination method begins the same as the previous one by finding those pixels where the value of the focus measure for a pixel exceeds a 40% threshold. The areas of selected pixels are then allowed to grow outwards by adding pixels at their edges that have the average frame number for surrounding pixels. This is continued until the areas coalesce and fill the whole image.

5.2 Image Comparison Techniques

Numerous Investigations and research has gone into the development and innovation of extended depth of focus algorithms. However, not a great deal has been invested into the quantitative comparison of the performance of the various algorithms and as such becomes the subjective qualitative appreciation of the user.

5.2.1 Mean Square Error

A common method of comparison is the mean-square error, or the root mean-square error. Calculation of the mean-square error involves squaring the difference of the acquired and desired value, summing over a series of these differences and dividing the total by the number of elements in the set. The calculation is shown below.

$$MSE=\frac{1}{m}\sum_{i=1}^{m}(x_i - T)^2$$

Where x_i i is the obtained value T is the target value. The result represents the deviation from the desired result. A MSE calculation on a set of values with no error yields a zero MSE.

5.2.2 Time to perform fusion

The time to perform the fusion process is used as a means of performing a comparison between the various algorithms. This is important as performing the process in minimum time and with the least amount of strain on the available system computational resources is of value.

5.2.3 Subjective Comparison

Finally, the images produced by any image fusion technique will be made us of by individuals who are not concerned about RGB values or algorithm complexity. What is of value to them is weather or not they believe the image shows them an acceptable amount of detail for their needs. Thus using a subjective comparison is a good way of testing if an algorithm lives up to expectations and therefore its performance.

Chapter 6

Comparison of Algorithm Performance

A Comparison of the performance of two of the algorithms analysed in chapter four above and whose implementation is discussed in chapter five is documented in this chapter.
In addition, these two implementations are tested up against a popular, freely available, program, *combineZ5*.

The algorithms were selected based upon the category, within which they fell, namely, Algorithm 1 from section 4.1.1 and Algorithm2 from section 4.2.1, as their complexity relative to that implemented by *combineZ5* is less. This serves not only to further the objectives of this thesis but to, in addition, mitigate the concerns raised in the background to the thesis in section 1.2. Therefore, the quality of the final image produced, measured by the techniques mentioned in section 5.2 Image Comparison Techniques above, and is weighted against algorithm complexity and computation time. Conclusions based on the analysis of the results herein ensue in chapter 7.
The images used to test the data have been obtained form various online sources. It is unfortunate that producing a data set of acceptable quality requires the use of expensive equipment. Moreover, it is a complex and laborious task as *motion blur, illumination variations and misregistration* are pertinent issues not easily avoidable.

That being said however, the image sets employed during this testing phase have been specifically chosen in an effort to test the three implementations in meaningful ways.

6.1 Data Set 1 Algae

The first set of images tested comprised of six images, of various focus, of algae. The set is shown below in Figure 21: Data set 1, Algae. The algae is made use of as this data set presents a straight forward challenge, it does not suffer from any optics related degradation and the subject matter does not contain an out of the ordinary amount of detail.

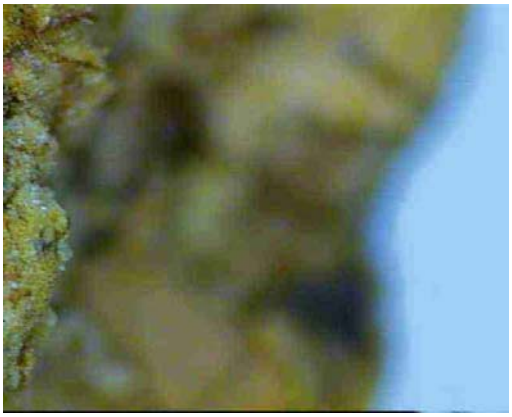

Algae 01

Algae 02

Algae 03

Algae 04

Algae 05

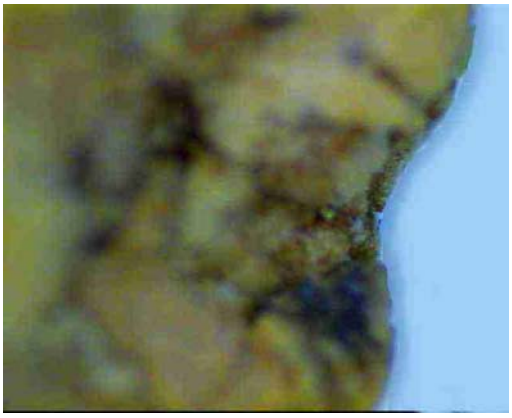

Algae 06

Figure 21: Data set 1, Algae

The result of the first algorithm follows below in Figure 22: Result of algorithm 1 on data set 1:

Figure 22: Result of algorithm 1 on data set 1

The result of the second algorithm follows below in Figure 23: Result of algorithm 2 on data set 1:

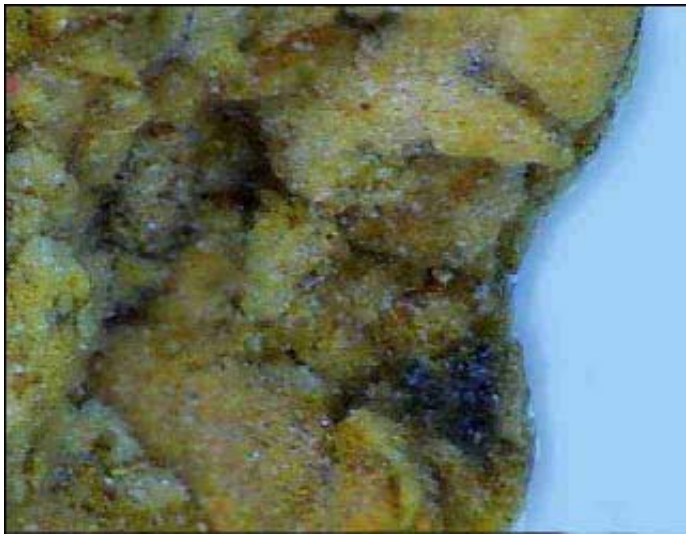

Figure 23: Result of algorithm 2 on data set 1

Finally data set 1 is tested with the application *combineZ5*, the result follows in Figure 24: Result of combineZ5 on data set 1, below:

Figure 24: Result of combineZ5 on data set 1

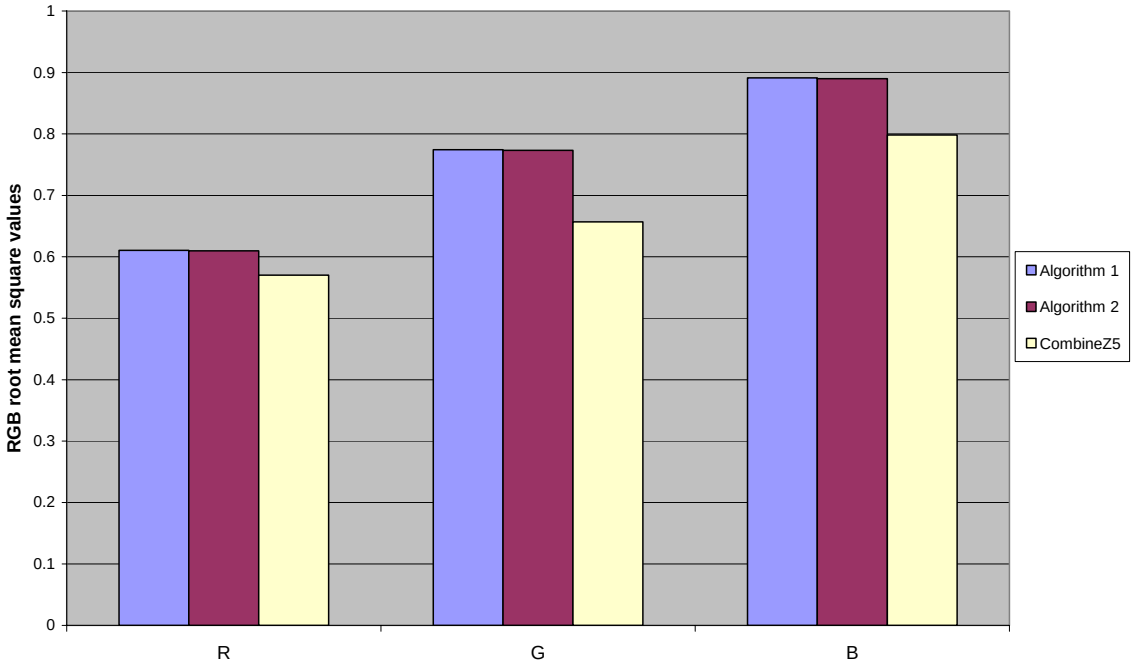

Figure 25: Graph comparing root mean square RGB values to each algorithm on data set 1

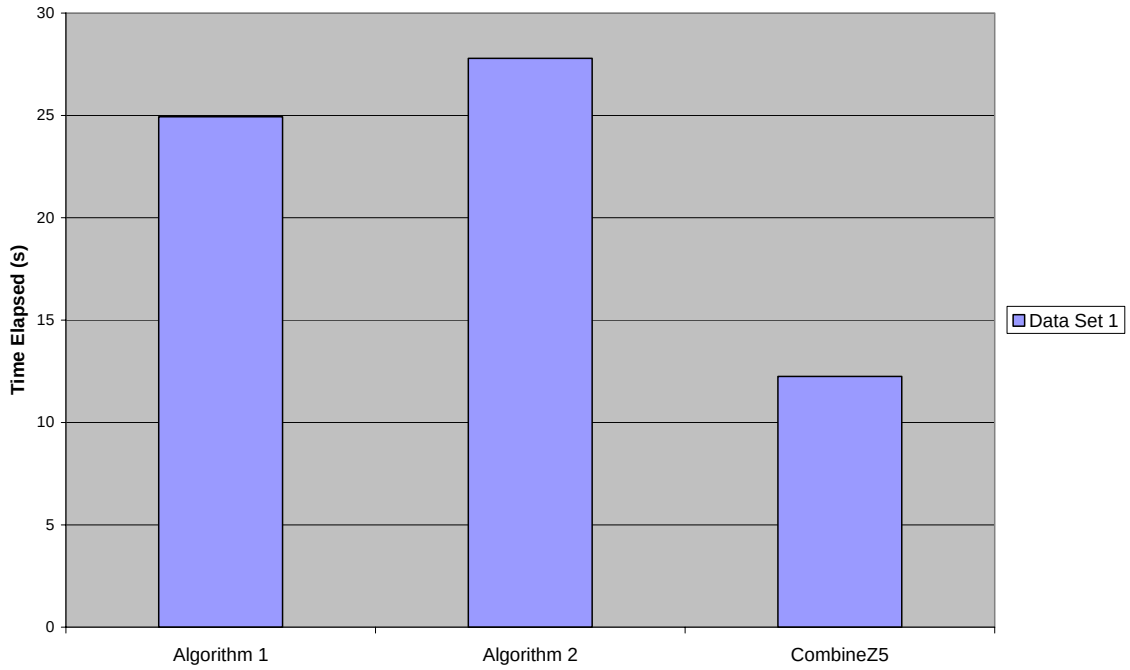

Figure 26: Graph comparing execution time of algorithms on data set 1

From the results presented it is seen that *CombineZ5* clearly produces the most desirable results, however, this comes as no surprise as *CombineZ5* is specialised and optimised software designed for this purpose. What is of interest however is that the RGB Root Mean Square (RGB RMS) values show that although combineZ5 does perform well, the performance of algorithm 2 is not far off. Furthermore, algorithm 1 reflects a similar performance to algorithm 2. Observing the resultant images pays testament to this observation. Moreover, not surprisingly algorithm two takes more time to compute than does algorithm one as its implementation is of a greater complexity. CombineZ5, although no doubt implementing the greatest amount of complexity performed the best time wise as well. As it is a package designed specifically for this application and is updated regularly, this can be accredited to the efficiency of its algorithms.

6.2 Data Set 2 Spider's Mouth Parts

The second set of images tested comprised of four images, of various focus, of a spider's mouth parts. The set is shown in Figure 27: Data set 2, parts of a spider's mouth, below.

This data set has been selected as the specimen is fairly translucent and not entirely opaque. This is of consequence as transparent specimens do not absorb light, but instead, produce a phase change of light. These specimens are invisible or very difficult to image because the human eye is insensitive to changes in the relative phase shifts of visible light waves.

SpiderMouth 01

SpiderMouth 02

SpiderMouth 03

SpiderMouth 04

Figure 27: Data set 2, parts of a spider's mouth

The result of algorithm 1 is shown below:

Figure 28: Result of algorithm 1 on data set 2

The result of algorithm 2 is shown below:

Figure 29: Result of algorithm 2 on data set 2

The result of *combineZ5* on data set 2 is shown below.

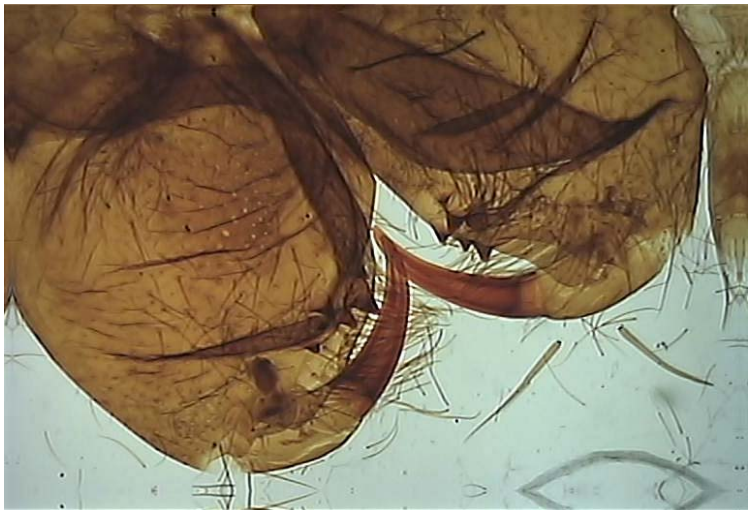

Figure 30: Result of combineZ5 on data set 2

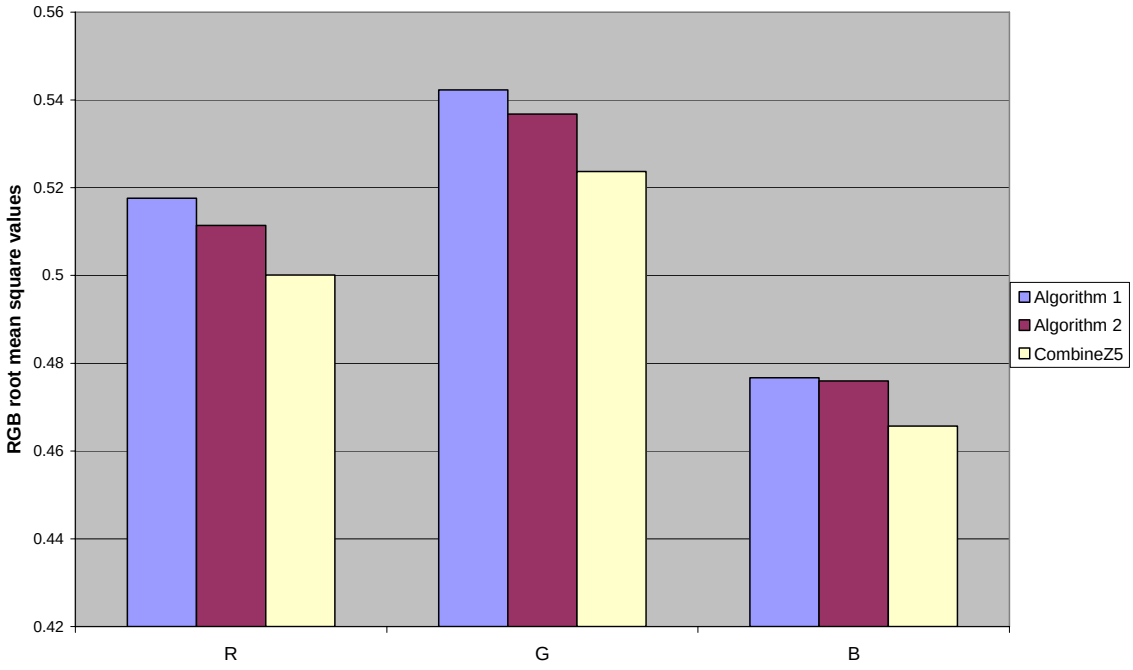

Figure 31:Graph comparing root mean square RGB values to each algorithm on data set 2

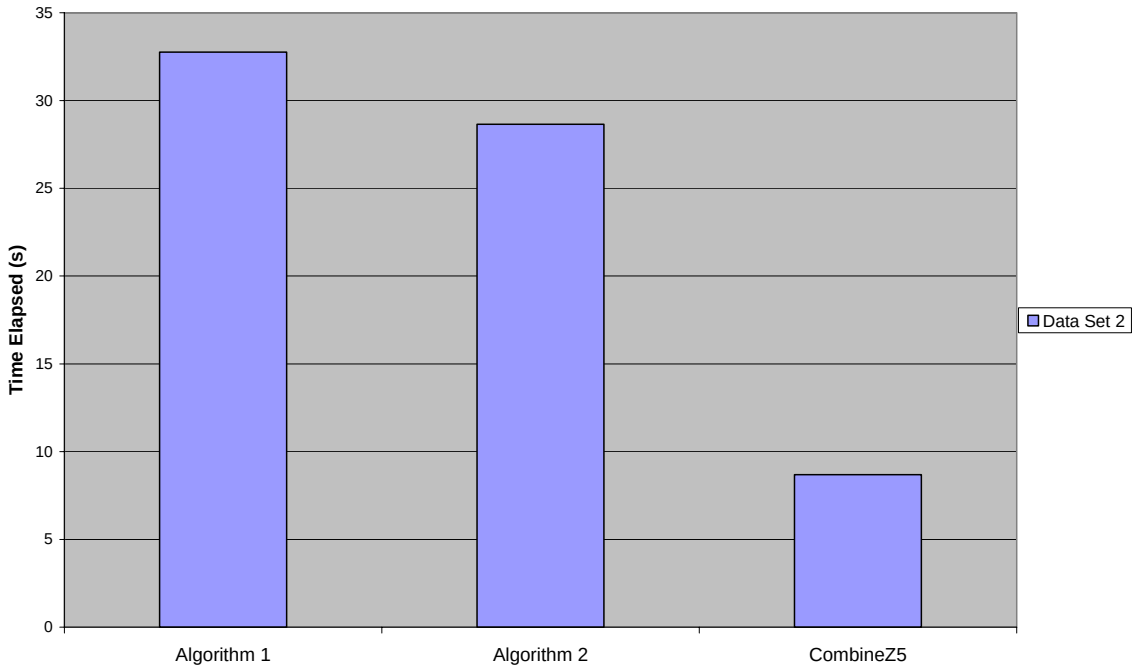

Figure 32:Graph comparing execution time of algorithms on data set 2

The results for the second data set do present the expected scenario. *CombineZ5* produces the most in focus image quantitatively and subjectively, Once more though the performance of algorithm 2 is not far behind that of *combineZ5*. The execution times though do present an interesting outcome. Algorithm 1, although using a simpler computational algorithm to algorithm 2, took a longer time to compute. This may be the case due to the size of the input images, although the number of images is reduced their resolution has increased and therefore, the number of iterative loops in the algorithm that are entered in order to deal with this increase grow, resulting in the increased computational complexity of algorithm 1.

6.3 Data Set 3 A Rock Surface

The third set of images comprised of five images of a rock, as depicted in Figure 33: Data set 3, part of a rock below: This data set has a certain monotonicity, which poses a problem for image fusion algorithms as areas of focus are difficult to distinguish and therefore discerning between them is a challenge.

Rock 01

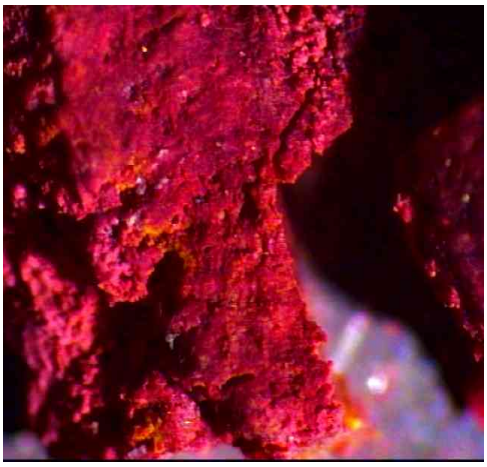

Rock 02

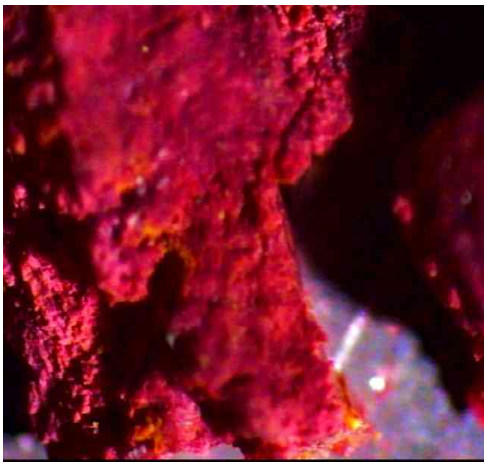

Rock 03

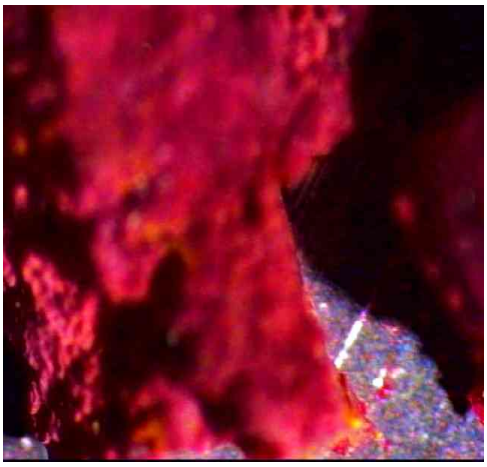

Rock 04

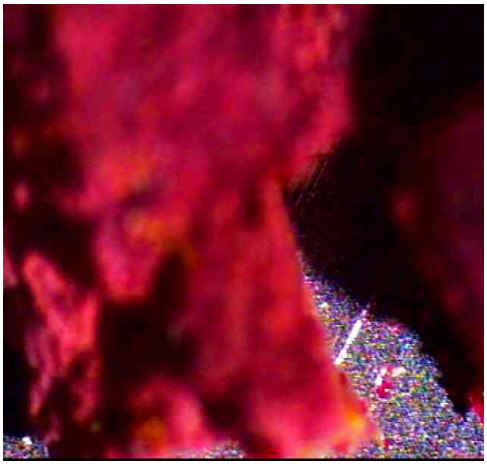

Rock 05

Figure 33: Data set 3, part of a rock

The result of algorithm 1 is shown below:

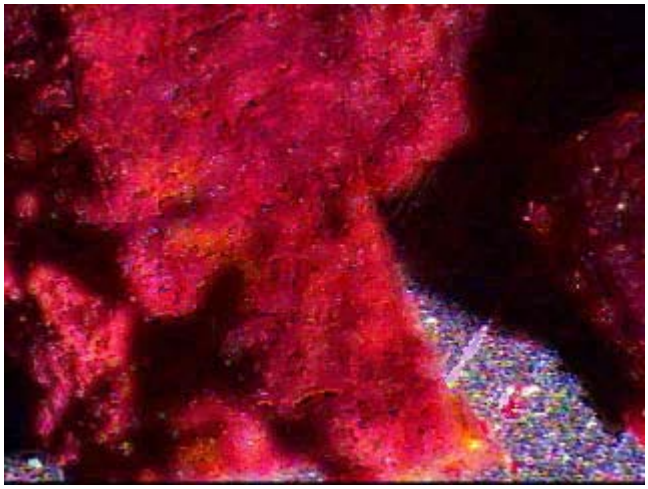

Figure 34: Result of algorithm 1 on data set 3

The result of algorithm 2 is shown below:

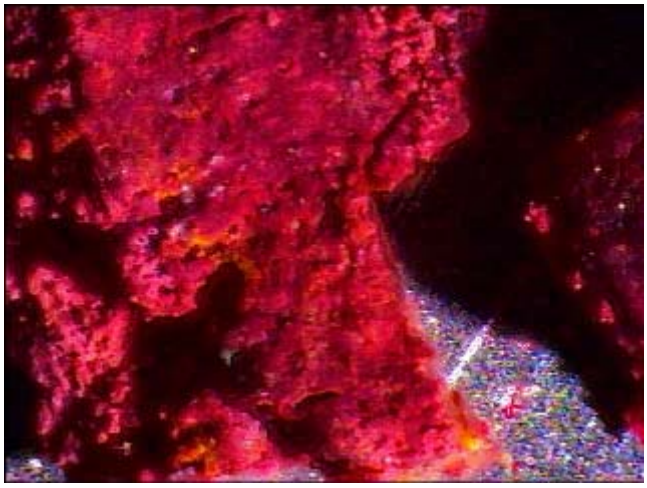

Figure 35: Result of algorithm 2 on data set 3

The result of *combineZ5* on data set 3

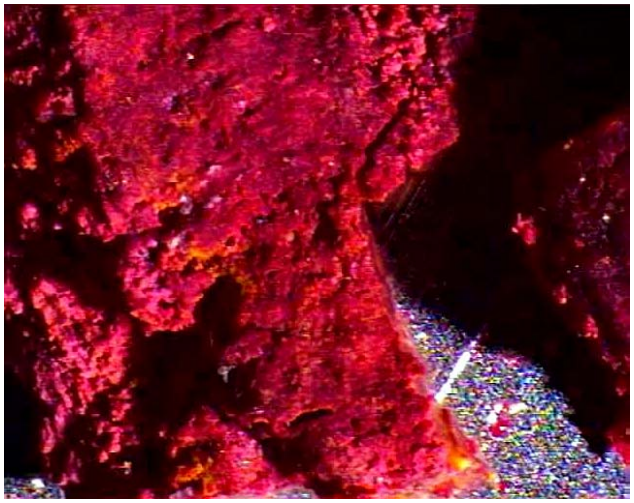

Figure 36: Result of combinez5 on data set 3

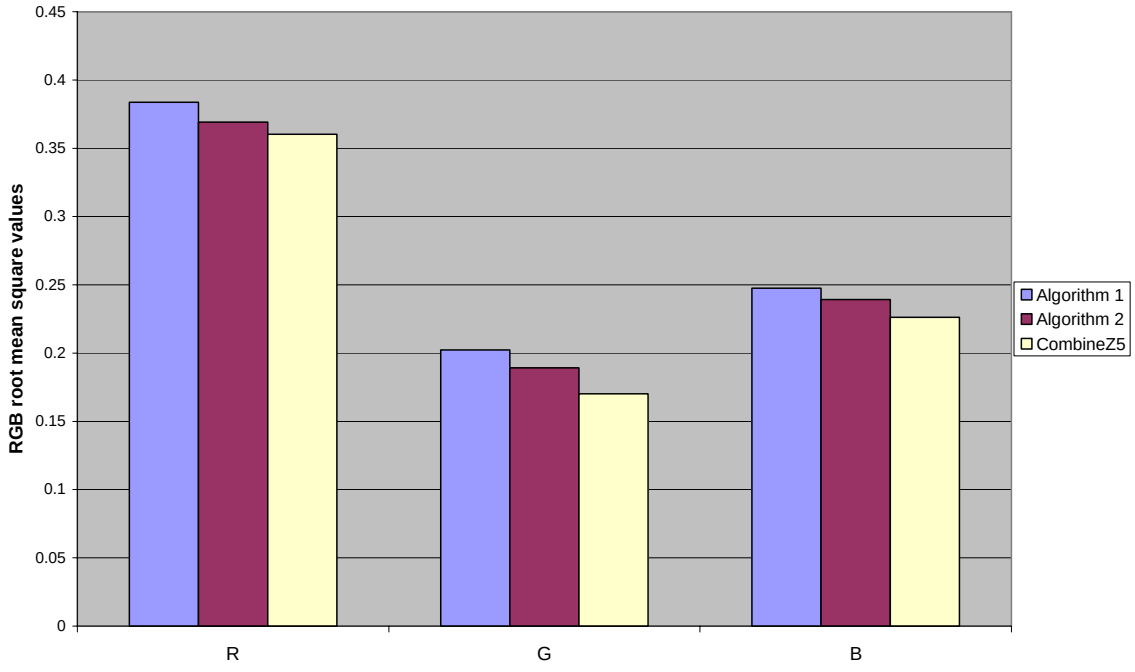

Figure 37:Graph comparing root mean square RGB values to each algorithm on data set 3

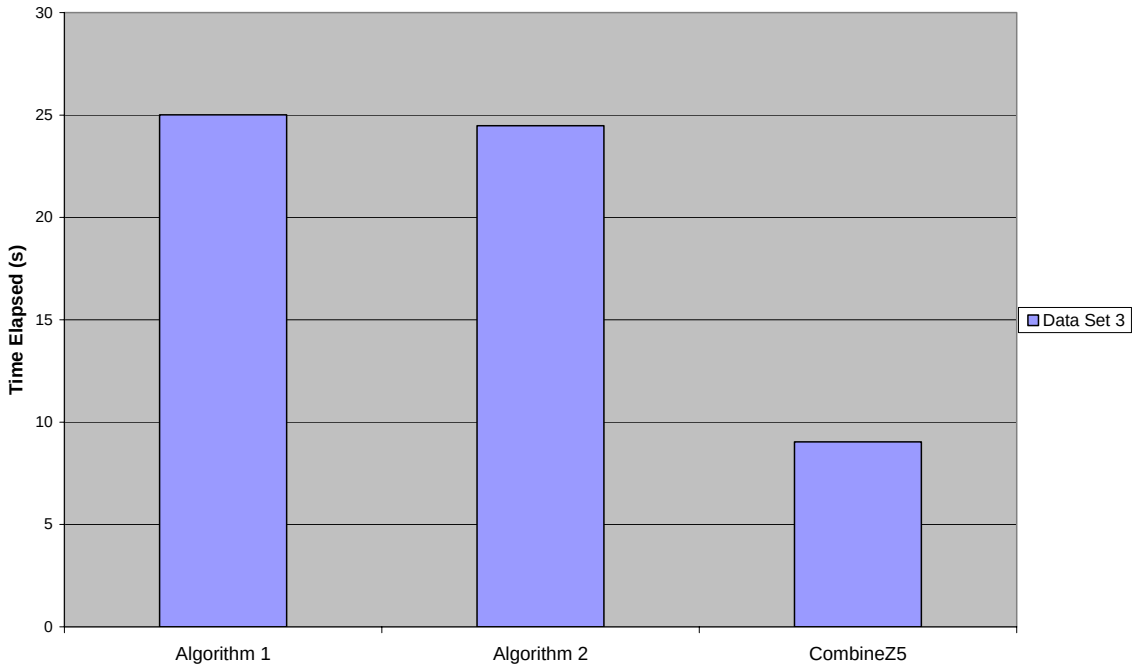

Figure 38:Graph comparing execution time of algorithms on data set 3

The results presented here solidify the trend that has been observed thus far. The combineZ5 software produces the better results; however the difference between the combineZ5 image and the image produced by algorithm 2 is hardly discernable. The image produced by algorithm 1 performs really poorly, suffering from the halo effect and failing to resolve the detail on the rock surface.

6.4 Data Set 4 A Spider

The final data set used comprises of four images of a spider body shown in Figure 39: data set 4 a spider's body below. This data set was chosen because of the level of detail on the spider's body making it an excellent test of the algorithm's ability to bring out finer detail.

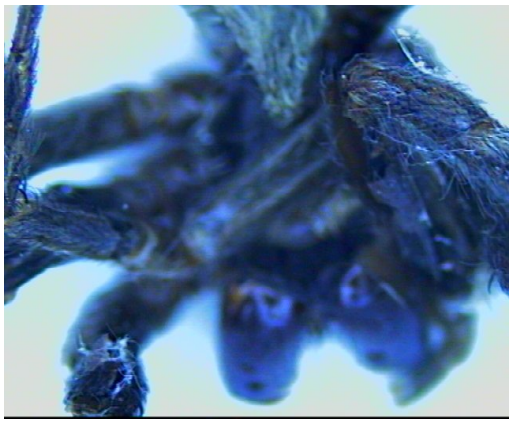

Spider Body 01

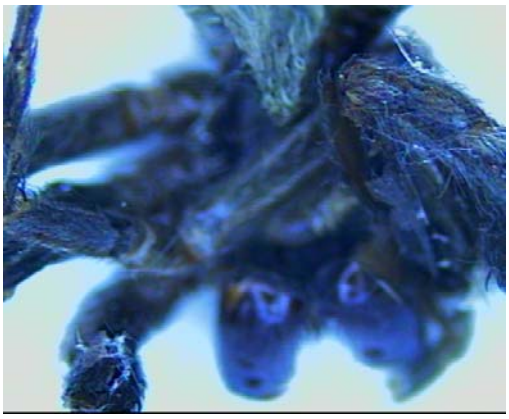

Spider Body 02

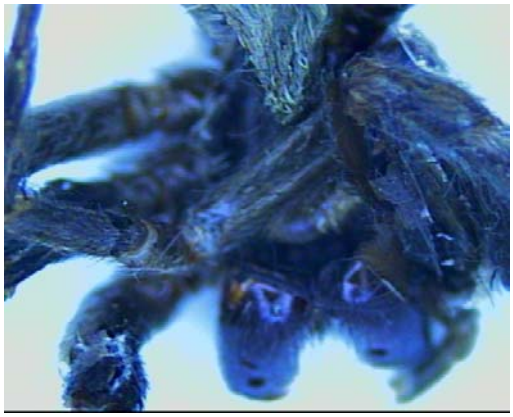

Spider Body 03

Spider Body 04

Figure 39: data set 4 a spider's body

The result of algorithm 1 is shown below:

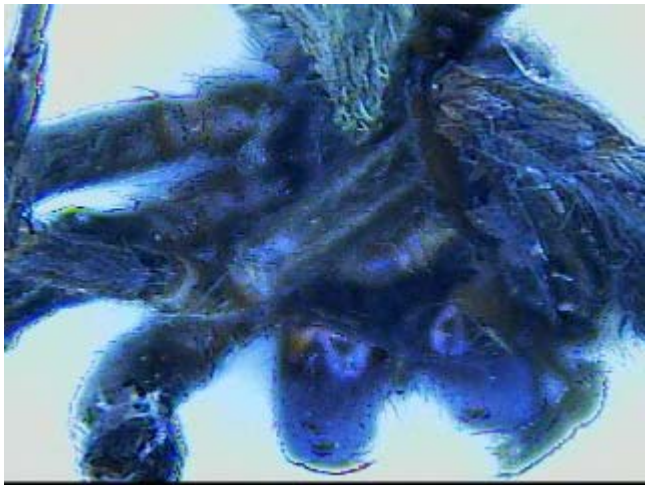

Figure 40: Result of algorithm 1 on data set 4

The result of algorithm 2 is shown below:

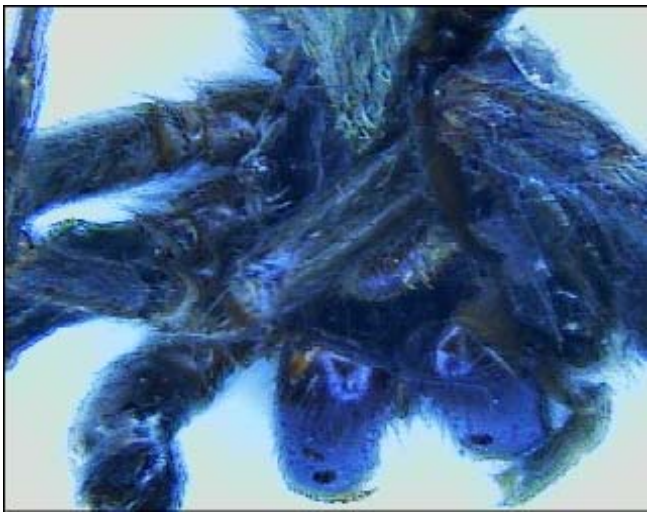

Figure 41: Result of algorithm 2 on data set 4

The result of *combineZ5* on data set 5.

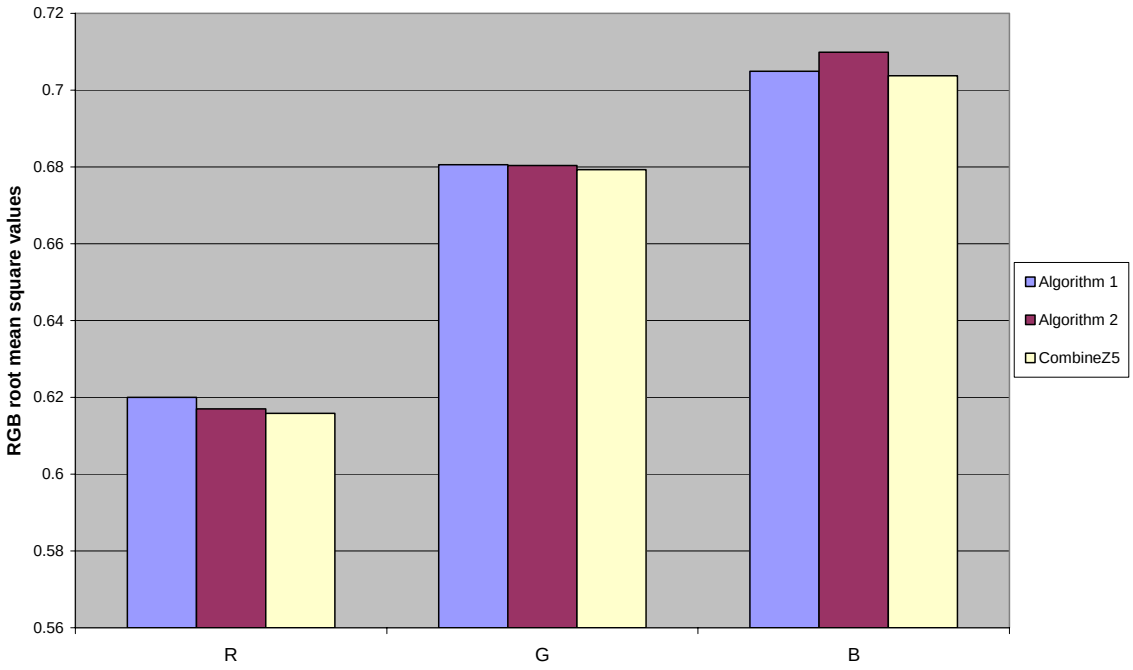

Figure 42:Graph comparing root mean square RGB values to each algorithm on data set 4

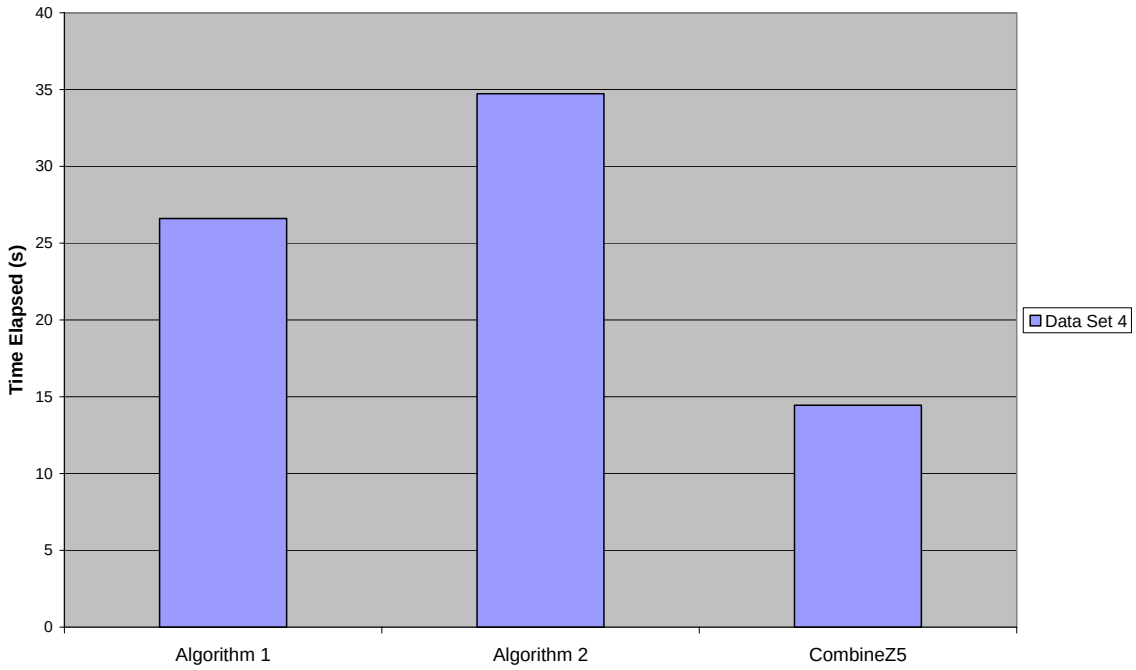

Figure 43: Graph comparing execution time of algorithms on data set 4

Once more we observe a dismal performance from algorithm 1, the final image is plagued by a combination effects, such as the 'halo' effect and mottling. The fine detail present in the image is not realised from the first algorithm. The RGB RMS values propose once more that combineZ5 produced the best focused image. Observing the final images there is little to distinguish between the results of algorithm 2 and combineZ5.
The execution time also performs as expected with algorithm 2 taking the greatest amount of type to complete its computation.

6.5 Subjective Appreciation Testing

In addition to the RGB RMS and computation time tests a subjective test was carried out that established the level of acceptability of the quality of the final reconstructed images. This was conducted by presenting twenty people with the three final images of each data set and ascertaining which of the images they believed were of a quality suitable to perform an objective scrutiny of the specimen. The results plotted were derived by

dividing the number of times an image from a certain algorithm was selected by the total number of times it could possibly have been selected. This is shown in the graph below.

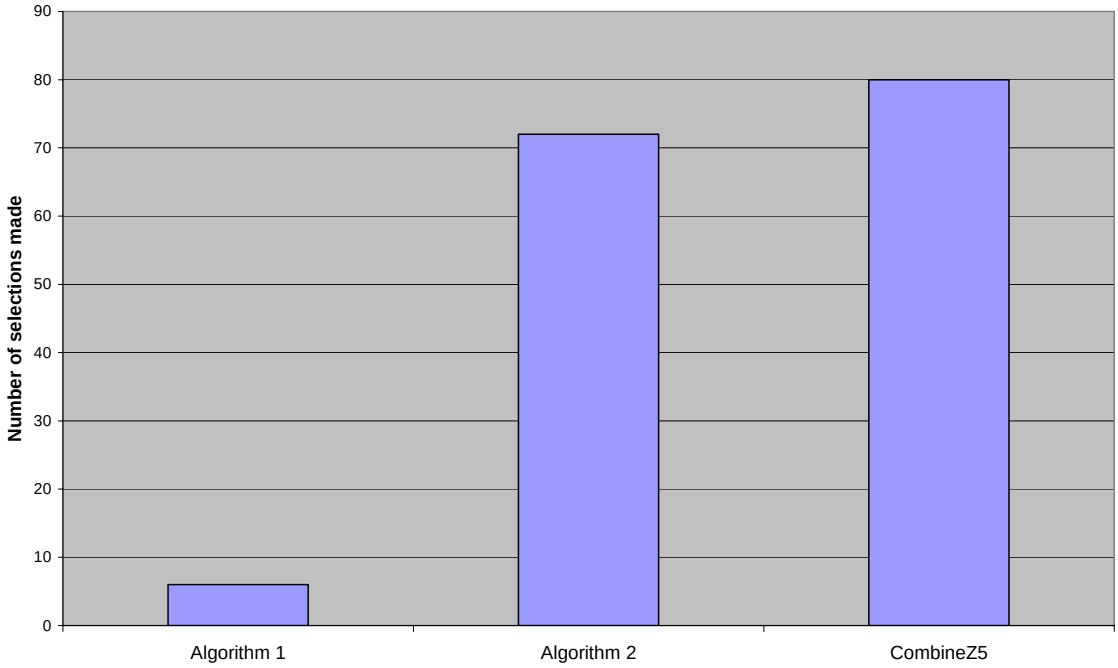

Figure 44: Result of subjective test

Chapter 7

Conclusions

This thesis investigates the performance of Algorithm 1 from section 4.1.1 and Algorithm2 from section 4.2.2 above, both implementations employ variance based methodologies, selected for their lack of complexity and relatively small time to compute. This performance is contrasted against *combineZ5,* a freely available image processing application designed to enhance Depth of field.

The purpose of such an investigation finds meaning against the backdrop provided by a world of continuous technological progression and the increased demand for ubiquitous data; anywhere, anytime with ease and very importantly at low cost.
Situations where this analysis is of consequence include lower level classrooms, veterinary or low cost health clinics, laboratory or home environments which could not otherwise afford high quality microscopes, machinevision or inspection and even biometric analysis. Portable and discrete devices will have power and resource constraints and thus algorithm complexity and efficiency are of concern.

Balancing these concerns yet maintaining an acceptable level of image quality is the challenge that is sought to be addressed.

From the results obtained in chapter 6 Comparison of Algorithm Performance above a number of conclusions are deduced.

- *CombineZ5* produces the best results

This is as expected as *CombineZ5* makes use of more sophisticated focus measure algorithms than the other two implementations tested. Furthermore, *CombineZ5* makes use of smoothing algorithms that remove undesirable artefacts from the final image. However, though that maybe the case, algorithm 2 produces results that come surprisingly close to matching those produced by *CombineZ5,* although it does not implement any smoothing algorithms.

As expected algorithm 1 does not perform as well as the other two, and in fact produces acceptable results only on the first data set. It suffers greatly from the visual effects associated with employing the simple maximum fusion rule mentioned above in 5.1.1 Simple Maximum such 'halos'.

- The most desirable results for time to compute are shown by *CombineZ5*.

Although *CombineZ5,* does have a greater algorithm complexity it out paces algorithm 1 and algorithm 2 for speed of performance. This is the case as *CombineZ5,* has been optimised specifically for this type of application, whereas algorithm 1 and algorithm 2 are mere lab implementations and thus have in efficiencies. That being said, it is of value to note that algorithm 2, with a greater complexity than algorithm 1, did perform its operation as expected in more time.

- Algorithm 2 is judged the most appropriate choice

From the results to the subjective test, it is noted that a high percentage of independent observers believe that algorithm 2 produces results of an acceptable quality.

Although, quantitatively, *CombineZ5,* does produce more desirable results the advantages that algorithm 2 has of possessing a smaller code footprint and a computationally less complex solution while maintaining comparable image quality are in keeping with the objectives and background to the investigation.

Chapter 8

Future Work

The scope and range of opportunity for innovation of the concept of extending depth of focus is broad. A plethora of applications and means to achieving those applications exist and require further work and investigation.

With regard to this specific project, a point of grave importance and concern for all systems, is that of image acquisition and registration. It can be the difference between producing high quality composite images and disastrous results.
Further research into techniques that deal with addressing this challenge need to be investigated. In addition, low cost imaging in order to support the idea of mobility provides an interesting dimension to the challenge of deep focus, considering the nature of the equipment required to perform the task. Further research toward this end would as well be valuable.

Alternative areas of interest that would benefit from further research include:

- 3D reconstruction of images from the multiple 2D images.
- Performing a deep focus moving images, such as is the case with bacteria for example
- Investigation into the use of stereoscopic vision as an approach to the challenge of addressing deep focus.

Chapter 9

References

[01] Helmy A. Eltoukhy, Sam Kavusi. A Computationally Efficient Algorithm for Multi-Focus Image Reconstruction, Department of Electrical Engineering, Stanford University (2003)

[02] Stuart Ball. Generating images with enhanced depth of field by creating a seamless mosaic from a sequence of images with different focal settings. (2004)

[03] Alan Boyde. Improved Depth of Field in the Scanning Electron Microscope Derived from through-Focus Image Stacks. Queen Mary, University of London 2004

[04] Forster B, Van de Ville D, Berent J, Sage D, Unser M. Complex wavelets for extended Depth of Field: A new Method for the Fusion of Multichannel Microscopy Images. (2004)

[05] Marshall D, Valdecasas A. G, Becerra J. M, Terrero J. J. On the Extended Depth of Focus algorithms for Bright Field Microscopy.

[06] Goldsmith N. Deep Focus; A digital image processing technique to produce Improved Focal Depth in Light Microscopy (2000)

[07] Agrawala M, Agarwala A, Salesin D, Drucker S, Colburn A, Cohen M, Curless B Dontcheva M. Interactive Digital Photomontage. ACM SIGGRAPGH (2004)

[08] Flannery W. H, Teukolsky B. P, Vetterling W.T, The Art of Scientific Computing. Numerical Recipes, Cambridge University Press, Cambridge, (1986)

[09] Parker J.R. Algorithms for Image Processing and Computer Vision, Wiley, New York (1997)

[10] Dowski E.R Jr., Johnson G.E. Wavefront Coding: A modern method of achieving high performance and/or low cost imaging systems (1995)

[11] Tucker S.C, Cathey W.T, Dowski E.R Jr. Extended depth of field and aberration control for inexpensive digital microscope systems (1998)

[12] Ferraro P, Simonetta G, Domenico A. Extended focused image in microscopy by digital holography, submitted to the optical society of america (2005)

[13] Kevin Willey, http://www.kevinwilley.com/l3_topic02.htm/, 18 October 2005

[14] http://www.cambridgeincolour.com/tutorials/depth-of-field.htm/, 18 October 2005

[15] http://en.wikipedia.org/wiki/Depth_of_focus/, 18 October 2005

[16] http://en.wikipedia.org/wiki/Aperture/, 18 October 2005

[17] http://en.wikipedia.org/wiki/Deep_focus/, 18 October 2005

[18] http://en.wikipedia.org/wiki/Depth_of_field/, 18 October 2005

[19] http://en.wikipedia.org/wiki/Focal_length/, 18 October 2005

[20] http://en.wikipedia.org/wiki/Focus_%28optics%29/, 18 October 2005

[21] http://en.wikipedia.org/wiki/Lens_%28optics%29/, 18 October 2005

[22] http://en.wikipedia.org/wiki/Circle_of_confusion/, 18 October 2005

[23] http://science.howstuffworks.com/camera2.htm/, 18 October 2005

[24] http://www.cs.mtu.edu/~shene/DigiCam/User-Guide/950/depth-of-field.html/, 18 October 2005

[25] http://www.ephotozine.com/techniques/viewtechnique.cfm?recid=63/, 18 October 2005

[26] http://www.jimbullard.org/sharp.htm/, 18 October 2005

[27] http://www.charfac.umn.edu/glossary/f.html/, 18 October 2005

[28] http://webster.commnet.edu/media/galleries/000920_Irish_Tradition/pages/motion%20blur-02.htm/, 18 October 2005

[29] http://www.microscopy-uk.org.uk/full_menu.html/, 18 October 2005

Appendix A

Results of Comparisons

A.1 Results of RGB root mean square calculation

Data set 1	R	G	B
Algorithm 1	0.6105	0.7743	0.8914
Algorithm 2	0.6096	0.7732	0.8899
CombineZ5	0.5701	0.6568	0.7982

Table 1:RGB root mean square values for data set 1

Data Set 2	R	G	B
Algorithm 1	0.5176	0.5423	0.4767
Algorithm 2	0.5114	0.5368	0.476
CombineZ5	0.5001	0.5237	0.4657

Table 2: RGB root mean square values for data set 2

Data Set 3	R	G	B
Algorithm 1	0.3837	0.2023	0.2475
Algorithm 2	0.3692	0.1892	0.2393
CombineZ5	0.3603	0.1702	0.2262

Table 3: RGB root mean square values for data set 3

Data Set 4	R	G	B
Algorithm 1	0.62	0.6806	0.7049
Algorithm 2	0.617	0.6804	0.7099
CombineZ5	0.6158	0.6793	0.7038

Table 4: RGB rot mean square values for data set 4

A.2 Results of time to compute measurements

	Algorithm 1	Algorithm 2	CombineZ5
Data Set 1	24.93	27.79	12.25

Table 5: Computation time of data set 1

	Algorithm 1	Algorithm 2	CombineZ5
Data Set 2	32.76	28.65	8.69

Table 6: Computation time of data set 2

	Algorithm 1	Algorithm 2	CombineZ5
Data Set 3	25.01	24.48	9.04

Table 7:Computation time of data set 3

	Algorithm 1	Algorithm 2	CombineZ5
Data Set 4	26.61	34.73	14.45

Table 8:Computation time of data set 4

A.3 Results of Subjective test

	Algorithm 1	Algorithm 2	CombineZ5
Number of times selected	6	72	80
Number of possible selections	80	80	80
Percentage popularity	7.5	90	100

Table 9: Results of subjective test